

# TRACERS OF CHROMOSPHERIC STRUCTURE I: OBSERVATIONS OF Ca II K AND H IN M DWARFS

Lucianne M. Walkowicz

Astronomy Department, University of Washington, Box 351580, Seattle, WA 98195-1580

Suzanne L. Hawley

Astronomy Department, University of Washington, Box 351580, Seattle, WA 98195-1580

Draft version February 21, 2024

## ABSTRACT

We report on our observing program<sup>1</sup> to capture simultaneous spectra of Ca II and Balmer lines in a sample of nearby M3 dwarfs. Our goal is to investigate the chromospheric temperature structure required to produce these lines at the observed levels. We find a strong positive correlation between instantaneous measurements of Ca II K and the Balmer lines in active stars, although these lines may not be positively correlated in time-resolved measurements. The relationship between H and Ca II K remains ambiguous for weak and intermediate activity stars, with H absorption corresponding to a range of Ca II K emission. A similar relationship is also observed between Ca II K and the higher order Balmer lines. As our sample consists of a single spectral type, correlations between these important chromospheric tracers cannot be ascribed to continuum effects, as suggested by other authors. These data confirm prior non-simultaneous observations of the H line behavior with increasing activity, showing an initial increase in the H absorption with increasing Ca II K emission, prior to H filling in and eventually becoming a pure emission line in the most active stars. We also compare our optical measurements with archival UV and X-ray measurements, finding a positive correlation between the chromospheric and coronal emission for both high and intermediate activity stars. We compare our results with previous determinations of the active fraction of low mass stars, and discuss them in the context of surface inhomogeneity. Lastly, we discuss the application of these data as empirical constraints on new static models of quiescent M dwarf atmospheres.

Subject headings: stars: late-type | stars: low-mass, brown dwarfs | methods: data analysis

## 1. INTRODUCTION

Radiation from the chromospheres of Sun-like stars comes primarily from the Ca II resonance lines in the blue and Ca II infrared triplet, the Fe II and Mg II resonance lines in the near UV, and the Balmer series of Hydrogen in the optical (Linsky et al. 1982; Foukal 1990; Reid & Hawley 2005). In M dwarfs, high surface gravity compresses the stellar atmosphere, leading to higher density chromospheres and particularly strong Balmer emission (Linsky et al. 1982). While the Ca II lines are the brightest emission lines formed in the of the Solar chromosphere, contributing a radiative loss of  $5 \times 10^6$  ergs cm<sup>-2</sup> s<sup>-1</sup> (Foukal 1990), the Balmer emission in M dwarfs is much larger than all other chromospheric lines, comprising  $10^{-4}$  of the bolometric luminosity at early types (Linsky et al. 1982; West et al. 2004). This fact, combined with the intrinsic faintness of M dwarfs in the blue, has made the red H line the primary diagnostic spectral feature of chromospheric activity in these stars. Many M dwarfs also have prominent Ca II resonance line emission (particularly Ca II K, which is unblended even

at low resolution (as opposed to Ca II H, which is blended with H<sub>2</sub>). The subset of these stars which also show H emission are designated "active" (dMe).

H and Ca II K are two of the strongest optical emission lines in active M dwarf chromospheres, responsible for cooling the atmosphere, balancing the magnetic heating, and determining the resulting equilibrium structure (Sundland et al. 1988; Mauas & Falchi 1994). Across the M spectral class, there is a range of emission strength in Ca II K, and a wide variety of both absorption and emission in H. H appears to trace hotter regions of the chromosphere ( $\sim 7000$  K), while Ca II K traces the cooler regions between the temperature minimum and  $\sim 6000$  K (Giammapa, Worden, & Linsky 1982; Cram & Mullan 1985; Walkowicz et al. 2009). Thus together, H and Ca II K offer complementary information on chromospheric structure.

The nature and relationship of the Ca II K and H lines in both active and inactive M dwarfs has been controversial. It may be that Ca II K and H are not only complementary but integral pieces of information, which separately cannot offer a true understanding of the processes they trace. One point of contention has been the "zero point" of chromospheric activity, or what defines the weakest existing chromospheres. Young et al. (1984) have argued that the zero point for chromospheric activity is defined by strong H absorption. In contrast, Staufer & Hartmann (1986) claim that those stars with the weakest chromospheres also have the weakest H absorption. In their scenario, H begins as a weak, purely photospheric absorption line, which (when the atmosphere

Electronic address: lucianne@astro.washington.edu

Electronic address: slh@astro.washington.edu

<sup>1</sup>This paper is based on observations obtained with the Apache Point Observatory 3.5-meter telescope, which is owned and operated by the Astrophysical Research Consortium. Some of the data presented herein were obtained at the W. M. Keck Observatory, which is operated as a scientific partnership among the California Institute of Technology, the University of California and the National Aeronautics and Space Administration. The Observatory was made possible by the generous financial support of the W. M. Keck Foundation.

sphere is subject to magnetic heating) first increases in absorption equivalent width, then decreases as it fills in with emission, then becomes a pure emission line. The implication of this scenario is that both stars with intrinsically weak chromospheres, and stars with moderate amounts of magnetic activity, may exhibit weak H absorption. Without additional chromospheric indicators, such as the Ca II K line, it is impossible to distinguish intermediate activity stars from inactive stars. In M dwarfs, the cold temperature minimum is largely transparent to H photons (Pettersen & Coleman 1981), so only a very weak H absorption line is produced in the photosphere (Cram & Mullan 1985) (thus we adopt those stars having weak H absorption ( $< 0.1\text{\AA}$ ) and weak Ca II K emission ( $< 0.1\text{\AA}$ ) as being representative of the "zero point" of activity in our sample).

Prior studies of the relationship between H and Ca II K (Robinson et al. 1990; Rauscher & Marcy 2006; Cincunegui et al. 2007) have routinely observed a positive correlation between these lines in active M dwarfs. However, both Robinson et al. (1990) and Cincunegui et al. (2007) have suggested that this observed correlation is due to a color effect (in other words, that the relationship between these lines observed in a sample of mixed spectral types is due to enhanced contribution from high continuum fluxes in earlier type stars. These authors argue that because time-resolved observations of Ca II K and H emission are not always positively correlated in individual stars, the positive correlation between instantaneous measurements of these lines is the result of their spectral type, rather than the properties of their chromospheres.

Observations of Ca II K and H provide an important "point of contact" in linking theory to actual M dwarfs. Previous efforts to study this relationship have often relied on observations from different epochs to provide measurements of both lines for a given star (Cram & Giammapa 1987; Houdebine & Stempeles 1997). In active M dwarfs, however, both Ca II K and H vary on timescales from minutes to decades. Therefore, measurements of lines obtained from non-simultaneous observations are not truly comparable, and any attempt to model them may shed no greater light than comparing lines in two totally different stars. Indeed nearly every previous study, observational and theoretical, cites non-simultaneous data as the chief source of uncertainty in observed relations, and recommends synoptic observations of a sample of M dwarfs (Cram & Giammapa 1987; Robinson et al. 1990).

Although many surveys have measured the Balmer lines of low mass stars, particularly H (e.g. the Palomar-Michigan State University Survey, or PMSU; Gizis, Reid, & Hawley 2002), the desired dataset of synoptic Balmer and Ca II K observations is sparse. The non-simultaneous observations taken in previous surveys, along with samples that span a wide range of M spectral types (and therefore a wide range in color and absolute magnitude), have left the relationship between these important chromospheric tracers ambiguous. To remedy this uncertainty, we have carried out an extensive observing program of H and Ca II K in nearby M3 dwarfs. By taking simultaneous data for a single spectral class, we are able to determine if the observed correlation between

these chromospheric tracers is due to a continuum effect, or to an actual relationship between these lines in active chromospheres. We also examine whether multiple observations of the Balmer and Ca II lines in an individual star are correlated over time in the same sense as single observations, and if not, how this behavior can be reconciled with instantaneous measurements of these lines in single observations of that same star.

We also compare these observations with previous determinations of the active fraction of low mass stars (West et al. 2004, 2008a), which have relied solely on the H line as an activity proxy, although it has been widely assumed that most M dwarfs possess some level of Ca II K emission. Using the Ca II K line as an additional activity measure, this survey will allow us to determine what fraction of stars deemed "inactive" on the basis of H absorption actually do have Ca II K emission and therefore belong to an intermediate activity population.

Additionally, we examine the proposed H behavior found by Staufer & Hartmann (1986), whereby H first increases in absorption depth prior to filling in and going into emission. The Staufer & Hartmann (1986) scenario was derived from non-simultaneous observations of a sample composed of cool stars of a relatively wide range of mass. Cram & Mullan (1985) reported some success reproducing these observations using very simple model chromospheres, consisting of a slab with a constant temperature and density. Using this simple model, Cram & Mullan (1985) predict a different slope for the filling in of the H line depending on whether the increase in equivalent width is due to an increased heating rate in a homogeneous chromosphere, or an increased filling factor of active regions in a laterally inhomogeneous chromosphere. If the filling in of the H line is evident in our observations, it will provide further constraints on how chromospheric structure changes with increased activity, as well as the role played by lateral inhomogeneity.

We are motivated to investigate surface inhomogeneity by the results of West et al. (2008a), who used the observed fraction of active stars per spectral type, along with a simple dynamical model of the Galaxy, to infer activity lifetimes for M dwarfs across the spectral class. A large increase in the activity lifetime occurs over the range of M3-M5, corresponding to the mass boundary where stars are believed to become fully convective ( $> 0.35M_{\odot}$ ; Reid & Hawley 2005; Chabrier & Baraffe 1997). The transition to full convection may mark a change from a Solar-type, rotationally-dependent magnetic dynamo, to a turbulent dynamo that may or may not depend strongly on rotation. The decline in activity in a given star over its lifetime may also indicate a change in how that star's activity is generated: objects of transitional mass (such as the M3 stars we examine here) may still possess some marginal radiative zone, though the majority of the star is characterized by deep convection. In this case, it is possible that during the star's youth the activity is dominated by a Solar-type dynamo, where the boundary of the convective and radiative zones is responsible for most of the field generation, though a turbulent dynamo is also at work. As the star spins down with age, the rotation-dependent dynamo declines, and the turbulent dynamo becomes the predominant means of field generation. Indeed, recent simulations of the magnetic dynamo in fully convective stars

by Browning (2008) show that the turbulence-generated  $\alpha$  field has both large- and small-scale features. The typical size of these  $\alpha$  field structures are related to the radius, with those generated deeper in the interior being larger than those near the surface. In addition, the large scale  $\alpha$  field in these fully convective models can be generated and sustained even though differential rotation (which plays such a key role in Solar-type dynamos) is eventually quenched by the  $\alpha$  field itself. Interestingly, although the Browning (2008) models are convective throughout, convection in the core is relatively weak, and most of the energy is transported via the radiation.

There is some precedence for this "dual-dynamo" scenario on the Sun, which possesses both a large-scale global  $\alpha$  field and a small scale magnetic component that seems to be independent of the global  $\alpha$  field. The gross magnetic features of the Sun are thought to be due to the dynamo that originates in the tachocline, but the magnetic  $\alpha$  field of the quiet Sun is likely generated by turbulent convective motions close to the stellar surface (Meneguzzi & Pouquet 1986; Dumey et al. 1993; Vogler & Schussler 2007). The chromosphere is a thin layer, dynamic but not convective, threaded by convection-twisted magnetic fields that form the quiet Sun magnetic network (Abbett 2008). Field generation by turbulence near the surface is not to be confused with theories of  $\alpha^2$  dynamos, which generate global scale turbulent fields, or with acoustic heating of the chromosphere. Although acoustic heating is bound to be at work wherever convective motion is involved, purely mechanical means apparently cannot fully account for the chromospheric and coronal emission in the Sun, and the heating due to these surface turbulent fields is most likely magnetic in nature (Bercik et al. 2005, 2006).

In the stellar atmosphere, the manifestation of this behavior may be surface inhomogeneity, where the chromosphere can be represented by two components: one corresponding to magnetically active plage regions related to the large-scale  $\alpha$  field, analogous to active regions on the Sun, the other component representing a basal, turbulence-driven chromosphere (Schrijver et al. 1989). Observations of the solar surface indicate that these inhomogeneities are complex indeed (Ca II K core emission corresponds spatially to regions of concentrated magnetic  $\alpha$  field, such as in active plage regions and bright network grains, while H  $\alpha$  absorption is produced in the both the mass of fibrils protruding from active regions, in mottles across the network of the quiet Sun and in enhanced emission from bright points during fares (Hasan & van Ballegoijen 2008; Rutten 2006, 2007). The diversity of structures in the solar chromosphere seems to indicate that even a dual component description is somewhat simplistic in nature (the magnetic features of a given star likely form a more continuous distribution, where the distinction between active and quiet areas is unclear (Schrijver 1988)). In the stellar case, however, we have no such detailed observations of surface inhomogeneities and must proceed cautiously with the number of free parameters we allow in our interpretation of spatially averaged spectra. However, if the Ca II or Balmer lines preferentially trace particular chromospheric components, examining their relationship may shed light on the nature of magnetic structures and the stellar dynamo in convective-boundary mass stars.

In the next section, we describe the observed sample. In Section 3, we discuss the observations and analysis, with particular attention to the effect of spectral resolution on interpreting relationships between chromospheric lines. In Section 4, we present the observed relationships between Ca II and the Balmer lines. We also place these observations in the context of previous surveys, addressing their implications for chromospheric structure. Lastly, we comment on our proposed theory of atmospheric inhomogeneity in light of the observations, and discuss future plans to test this proposition with a new suite of non-LTE model atmospheres.

## 2. THE SAMPLE

Our sample consists of 81 stars in the Palomar/M SU Nearby Star Spectroscopic Survey (PM SU; Reid, Hawley & Gizis 1995; Hawley, Gizis & Reid 1996; Gizis, Reid, & Hawley 2002; Reid, Gizis & Hawley 2002) of the same approximate spectral type, M 3V (see Table 1 for a summary of our sample stars). The PM SU Survey determined spectral types based on a set of spectroscopic indices for TiO and CaH (see Reid, Hawley & Gizis 1995, for details). Our sample is also quite homogeneous in color, having a median Cousins V-I = 2.55  $\pm$  0.12 (corresponding to a difference in  $T_{\text{eff}}$  of roughly 50K; Reid & Hawley (2005)). The PM SU Survey H  $\alpha$  measurements enabled us to select a sample that is representative of varying levels of chromospheric activity, from very weak H  $\alpha$  absorption (indicating either a weak or intermediate strength chromosphere), to powerful emission (indicating strong chromospheric activity). Limiting the spectral range of our objects is important, as it has been noted (Staufer & Hartmann 1986; Rutten 1987) that the relation between the chromospheric flux in the Ca II K line and the equivalent width in H  $\alpha$  depends on the spectral type of the star (i.e. the stellar continuum flux). Previous studies have attempted to correct for this effect by binning their measurements by stellar color (Robinson et al. 1990). By limiting our sample to a single spectral class, we are able to examine the relation between Ca II K and H  $\alpha$  without having to disentangle systematic trends with color and spectral type. Although many of the stars we observe have existing optical data, our new data comprise simultaneous observations of both lines at comparable resolution.

## 3. OBSERVATIONS AND ANALYSIS

Data were obtained with the ARC 3.5m Telescope at Apache Point Observatory (APO), using the Dual Imaging Spectrograph (DIS) and the ARC echelle spectrograph (ARCES). Additional high resolution data (HIRES) were available for many of our stars from the California Planet Search (CPS; Butler et al. 1996; Wright et al. 2004). While the DIS spectra provide reliable flux information for our lines of interest, the echelle spectra enable an examination of the detailed line profile. High resolution data are particularly important for identifying intermediate activity objects, whose Ca II K chromospheric emission cores may not be resolved in the lower resolution spectra. Figure 1 shows example HIRES and DIS spectra for three stars of different activity levels. In the highly active star (top row: AD Leo), the H  $\alpha$  and Ca II K lines are quite clearly in emission in both the echelle and low resolution spectra, indicating

the presence of substantial chromospheric heating. The moderate activity example (middle row: G1362) shows very little H emission, but still has a noticeable Ca II K emission line. In the weakly active example (bottom row: GJ1125), the H line is in absorption and Ca II K emission is not evident in the low resolution spectrum. Based on its H line, this star would be classified as "inactive". However, the echelle spectrum of this star illuminates the importance of high resolution observations (even the "inactive" object possesses a noticeable Ca II K emission core when examined in detail. In the following subsections, we describe the observations, data reduction, and method of line measurement for the DIS and echelle spectra. We also compare high and low resolution measurements of the same stars, to investigate what biases may be introduced by the choice of spectral resolution.

### 3.1. DIS spectra

DIS is a low dispersion spectrograph with two cameras fed by a beam splitter, allowing blue and red spectra to be obtained simultaneously. Our data were taken using a 1<sup>st</sup> slit in combination with the higher resolution gratings, which have a dispersion of 830.8 lines mm<sup>-1</sup> on the red side (giving a dispersion of 0.84 Å pixel<sup>-1</sup>, R = 3200) and 1200 lines mm<sup>-1</sup> on the blue side (giving a dispersion of 0.62 Å pixel<sup>-1</sup>, R = 2000). Spectra typically covered the wavelength regions of 3700 Å to 4400 Å in the blue and 5600 Å to 7100 Å in the red.

The DIS data were reduced using standard IRAF reduction procedures (Massey et al. 1992). Data were bias-subtracted and flat-fielded, and one-dimensional spectra were extracted using the standard aperture extraction method. A wavelength scale was determined for each target spectrum using H&N&Ar arc lamp calibrations. Flux standard stars from Oke (1990) were observed each night and used to place the DIS spectra on a calibrated flux scale.

### 3.2. Echelle Spectra

The ARC echelle spectrograph (ARCES) captures the entire visible spectrum (roughly 3800 Å to 9800 Å) with a resolution of R = 31,500. While this resolution is high enough that even small Ca II K emission cores can be measured from our spectra, it does not fully resolve the Ca II K line profile, and thus information regarding the presence or lack of a central reversal in the detailed line profile (an important tracer of NLTE effects in the upper chromosphere) is lost in these spectra. Cosmic rays were removed from the raw echelle images, which were then bias-subtracted and flat-fielded. Scattered light in the ARCES spectra was removed to the 6-8% level using the apscatter task in the IRAF echelle package, which fits a two-dimensional surface to the dispersed and cross-dispersed interaperture light. One-dimensional spectra were extracted for data and ThAr arc lamp images. The ThAr arc lamp spectra were then used to determine the wavelength scale for each target spectrum using ThAr arc lamp spectra.

The CPS spectra were taken using the HIRES spectrograph on Keck I (R = 57,000; Vogt et al. 1994), and cover the wavelength regime of 3645–7990 Å. The Keck HIRES data were reduced using the Planet Search Re-

duction Pipeline, described in Wright et al. 2004 and Rauscher & Marcy (2006). The pipeline removes scattered light from the raw spectra by fitting a smooth function to counts lying between the orders, and subtracting this level from the raw data. This method removes the scattered light to 0–1 photon (G. Marcy, private communication). Equivalent widths for these objects have also been reported in Rauscher & Marcy (2006) and West et al. (2006), but we have remeasured them as part of our analysis to ensure consistency.

### 3.3. Measurement of Ca II K and Balmer Lines

The observed line profiles are a superposition of the photospheric and chromospheric contributions. In the case of the Ca II K line, the chromospheric emission core is easily identifiable in our echelle spectra even for stars with low activity levels, and so the two components of the line can be disentangled. As the distinction between photospheric and chromospheric contribution to the Balmer lines is considerably more ambiguous, we measure the entire (photospheric + chromospheric) line. Measuring the entire H line enables direct comparison between our work and previous studies that use H as an activity indicator, where traditionally no distinction has been made between the chromospheric and photospheric contributions to the line.

The Ca II K line was measured in the same way for both the HIRES and ARCES echelle data as well as the low resolution DIS data. As the Ca II K line profile contains both contributions from the chromospheric emission and the photospheric absorption, it is necessary to correct for the photospheric contribution in order to study the chromospheric emission itself. In order to remove the photospheric contribution to each line, we use a radiative equilibrium NextGen model atmosphere (log g = 5, T = 3400 K, solar metallicity; Hauschildt et al. 1999) with the NLTE radiative transfer code RH<sup>+</sup> (Uitenbroek 2001) to calculate the photospheric Ca II K line profile. The calculated line profile was normalized and scaled to match the continuum near the Ca II K line for each star. The model photospheric line profile was then overplotted with the observed data, and a line integration region was interactively chosen to include only the chromospheric emission; this method is illustrated in Figure 4. As the stars in our sample are all the same spectral type, the same model profile is used in each case and the correction is applied in the same way to each spectrum.

The total area under the interactively chosen region is then integrated both for the observed spectrum and the radiative equilibrium model. The flux above the radiative equilibrium model is taken as the chromospheric flux, and divided by the mean continuum level measured from a relatively featureless portion of the nearby spectrum to yield the equivalent width of the line (a summary of the wavelength regions chosen for the mean continuum and line integration regions is given in Table 2). We compare the results obtained with photospheric correction for objects with both echelle and DIS spectra in the next section.

As the Balmer lines have relatively simple profiles compared to the Ca II K line, such a detailed method of measurement was not necessary. They were instead measured using an automated method that sums the flux in rectan-

gular passbands, using a fixed integration region for each line. The Balmer lines in the DIS spectra were measured using the same fixed integration and continuum regions as for the high resolution observations (specified in Table 2).

As the lower resolution DIS spectra are flux calibrated, fluxes for the lines could be measured in addition to equivalent widths. Where given, surface fluxes were calculated using distances from PMSU (derived from the  $M_V - T_{\text{eff}}$  spectroscopic parallax relation, and calibrated against those stars in the sample possessing trigonometric parallaxes; see Gizis, Reid, & Hawley 2002) and a typical radius for an M3V star ( $2.85 \times 10^{10}$  cm; Reid & Hawley 2005).

Table 3 provides the line fluxes and equivalent widths for the entire sample as measured from the low resolution DIS spectra, while Table 4 provides equivalent widths measured for the subset of stars with echelle observations.

### 3.4. Comparison Between Low Resolution and Echelle Data

The detailed profiles from our echelle spectra enable us to easily disentangle the photospheric and chromospheric components of our lines, which is particularly important for stars with low levels of activity (and thus ambiguous low resolution spectra). We use the comparison between the equivalent widths measured from the low and high resolution spectra with photospheric correction to calibrate the effect of spectral resolution on our results.

Figures 2 and 3 compare the equivalent widths obtained from the DIS spectra with those from the echelle spectra. For low levels of activity, the Ca II K equivalent widths derived from the corrected low resolution data are a decent match with those derived from the high resolution data. The difference in equivalent widths calculated from the ARCES spectra versus the DIS spectra are 0.70Å in H and 1.11Å in Ca II K, while equivalent widths measured from the HRES spectra are 0.17Å in H and 0.18Å in Ca II K. However, as the activity of the star increases, equivalent widths calculated from the low resolution data are a good deal higher in both Ca II K and H: in H, the equivalent widths measured from ARCES spectra of active stars are 2.13Å lower than those measured from the low resolution spectra, while HRES measurements are 0.99Å lower. In Ca II K the effect is more pronounced, with the equivalent widths measured from ARCES and HRES spectra being 1.63Å and 3.73Å lower, respectively.

As our echelle spectra are not flux calibrated, the continua have subtle differences in slope compared to the continua of the DIS spectra. While this effect is small for the majority of the sample, which have small H equivalent widths, it becomes much more noticeable when the line is in emission and contains considerably more flux. In the case of the HRES spectra, H falls very close to the edge of the reddest order, and there is no adjacent order with which to join it. In both the HRES and ARCES spectra, the equivalent widths calculated from the echelle spectra are smaller than those calculated from the DIS spectra.

The differences between the two datasets indicate that equivalent widths calculated from high resolution data will be smaller for both the H and Ca II K lines in ac-

tive stars. Therefore, measurements taken from the high resolution spectra will be offset in their absolute values of the equivalent widths for the same star. However, comparisons between the high resolution measurements of H and Ca II K will show the same relationship as for the low resolution data due to the net effect being in the same direction for both lines. If correction for the photospheric component of the Ca II K line is not performed, however, the activity level will always be underestimated, especially for low activity objects whose emission cores are not resolved. In the following section, we only compare data of comparable resolution.

## 4. RESULTS

In this section we present our results and interpret them in response to the questions raised in the Introduction.

### 4.1. The Relationship Between H and Ca II K with Increasing Activity

Comparison of the Balmer and Ca II lines reveals a number of interesting relationships. Figure 5(a) plots the equivalent width of H versus the equivalent width of Ca II K as measured from our DIS spectra. The Ca II K line has been corrected for the photospheric component as described in Section 3, so the equivalent widths cited here represent the purely chromospheric contribution to the line. For the most active stars (those with H in emission, indicating strong chromospheric heating), the H and Ca II K equivalent widths are clearly correlated and increase monotonically, with increased scatter for stronger line strength. A linear fit to the H and Ca II K equivalent widths for the active stars yields an RMS deviation of 0.38Å, with stars of Ca II K equivalent width of less than 5.35Å<sup>1</sup> having an RMS deviation of 0.21Å, while the most active stars ( $EW_{\text{Ca II K}} > 5.35\text{Å}$ ) have an RMS deviation of 0.56Å. As these data are measured from a homogeneous sample of stars of the same spectral type, and the observations of Ca II K and H are simultaneous, the increased scatter is likely intrinsic and suggests a mild decoupling of the line behavior in the strongest chromospheres. Stars possessing weak to intermediate chromospheres cluster in the lower left corner of the plot, and are spread over a wide range in Ca II K for a relatively small range in H. These weakly active stars, plotted at an expanded scale in Figure 5(b), do not show any obvious correlation between the H and Ca II K equivalent widths. That a range in Ca II K emission strength can be associated with either deep or shallow H absorption lines lends credence to the Staufer & Hartmann (1986) scenario, where the photospheric H absorption line fills in with chromospheric emission as activity increases. However, an initial deepening of H absorption as Ca II K increases, suggested by Cram & Giampa (1987) and Staufer & Hartmann (1986), is not obvious in these low resolution observations.

<sup>1</sup> This value corresponds to the mean of the Ca II K equivalent widths measured for active stars and is a largely arbitrary choice for the division between "active" and "very active". Our result that the scatter increases with increasing activity is fairly insensitive to this value, routinely yielding an RMS deviation for the most active stars that is roughly twice that for less active stars.

Figure 5(b) illustrates the number of stars that would traditionally be classified as "inactive" based on having  $H$  in absorption, which actually do possess some chromospheric activity (indicated by their Ca II K emission). Of the 81 stars in our sample, 46 stars were classified as inactive based on having  $H$  in absorption; with the additional information provided by our Ca II K measurements, we find that all but possibly 1 of these stars have at least a low level of Ca II K emission. As discussed in the introduction, this result implies that  $H$ -based measurements of the active fraction in early M dwarfs (above the fully-convective mass boundary) may trace what fraction of stars have a solar-type magnetic component that relies on the presence of a radiative-convective zone boundary (the tachocline). However, as  $H$  emission is not only present but increasingly common in very low mass, fully convective M dwarfs which do not possess a tachocline,  $H$  in these stars may be associated with a global turbulent dynamo and thus trace an altogether different source of magnetic activity (as discussed in the Introduction).

Figure 6(a) shows echelle equivalent widths of the Ca II K chromospheric emission cores against the full (photospheric + chromospheric) equivalent width of the  $H$  line as a comparison with Figure 5(a). Figure 6(b) provides a similar comparison to the low activity stars as Figure 5(b). As in Figure 5(a), Figure 6(a) shows a very small variation in  $H$  absorption for a range of Ca II K emission. Figure 6(b) is intriguing, however, as the U-shape locus of points does seem to indicate an initial deepening of the  $H$  absorption line prior to its filling in and going into emission. This relationship was also observed by Rauscher & Marcy (2006) in their analysis of Ca II K HRES data and  $H$  equivalent widths from Gizis, Reid, & Hawley (2002) for M dwarfs of mixed spectral types, but the trend persists if we examine a homogeneous sample. A row of points indicating the approximate placement of the locus predicted by Cram & Giamfapa (1987) are shown with the data to guide the eye. The maximum  $H$  absorption equivalent width is  $-0.35\text{\AA}$ , which is consistent with the range observed by Staufer & Hartmann (1986). The maximum in  $H$  absorption seems to occur at roughly  $0.4 - 0.5\text{\AA}$  Ca II K equivalent width, suggesting that stars having Ca II K emission at this level and above have passed some critical threshold for the onset of  $H$  emission.

#### 4.2. Chromospheric Coupling: Surface Fluxes and Higher Order Balmer Lines

In Figure 7, the  $H$  equivalent width is plotted against the chromospheric Ca II K surface flux for our DIS sample. For M stars with  $H$  in absorption, a relatively small variation in  $H$  equivalent width corresponds to a wide range of Ca II K emission, confirming the results of Figure 5(a) above. For the strongest chromospheres, the decoupling of Ca II K and  $H$  emission suggested by Figure 5(a) is much more evident, with strong Ca II K flux being associated with a wide range of  $H$  emission strengths. These results confirm those of Robinson et al. (1990), although their analysis was complicated by the spread in spectral type of their sample (early K to mid M). They similarly corrected the Ca II K for the photospheric contribution to the equivalent width, but used a solar model scaled to the various temperatures of their

sample stars.

Figure 8 shows the relationship between the equivalent width of Ca II K and those of  $H$ ,  $H$ ,  $H$  and  $H\delta$ . As in the case of Figure 5(a), the equivalent widths are calculated from single DIS observations of our sample stars. Our results provide an interesting comparison to West et al. (2006), who reported that in multiple observations of the Balmer and Ca II lines in a given star, the higher order Balmer lines and Ca II H and K lines trace one another, while  $H$  varies seemingly randomly. From this plot, it is evident that the higher order Balmer lines follow Ca II K in a similar way to  $H$ . In contrast, Figure 9 (reprinted here from West et al. 2008b) shows the Balmer and Ca II K line equivalent widths measured from repeat echelle observations of AD Leo. Confirming the observation of West et al. (2006), we see that while the higher order Balmer lines vary little in relation to Ca II K ( $EW_H = 0.16\text{\AA}$ ;  $EW_H = 0.15\text{\AA}$ ;  $EW_H = 0.12\text{\AA}$ ), the  $H$  equivalent width can vary dramatically over time ( $EW_H = 0.57\text{\AA}$ ). Taken together, Figures 5(a), 8, and 9 imply that while the emission in Ca II K and the Balmer lines are positively correlated when measured from a single observation of a given star, they are not necessarily positively correlated over multiple observations of that star. In other words, more active chromospheres produce greater emission in both Ca II K and the Balmer lines overall, but  $H$  and Ca II K do not always trace one another directly in time-resolved measurements.

#### 4.3. Investigation of Continuum Effects

Although our sample is comprised of stars of the same spectral type, our stars cover a range of 2 magnitudes in  $M_V$ . As previous studies by Robinson et al. (1990) and Cinunegui et al. (2007) have suggested that the positive correlation between Ca II and the Balmer lines in active stars is due to enhanced continua in early spectral types, we investigated the possible relationship between absolute magnitude and activity indicators for our sample. Figure 10 shows the continuum fluxes near  $H$  and Ca II K versus the absolute V magnitude, while Figure 11 shows the equivalent widths of  $H$  and Ca II K versus absolute V magnitude. The absence of any relationship between absolute magnitude and the level of either activity or continuum flux shows that the positive correlation we observe between  $H$  and Ca II K in active stars cannot be ascribed to a continuum effect.

#### 4.4. Interpretation

A possible interpretation of these results is that the Ca II K and  $H$  fluxes observed are due to a laterally inhomogeneous atmosphere. Stated simply, increased activity leads to stronger emission in all lines, but does not imply that these lines trace the same source of activity or the same regions on the star. In analogy to the "zebra effect" suggested by Pettersen et al. (1992) to describe photometric variation on BY Dra stars, one may picture the stellar atmosphere as consisting mostly of a cooler "basal" chromosphere, heated either acoustically, through a weak, pervasive magnetic field, or some combination of the two. Stars with greater activity may have, in addition to this basal chromosphere, hotter active regions where magnetic flux tubes thread through the stellar atmosphere, analogous to bright plage regions on the Sun.

The stronger the stellar magnetic field, the more area of the stellar surface is covered by these active regions. The observed line profiles are a superposition of the line profiles produced by these two atmospheric components.

The Ca II K emission core responds linearly with increased activity (more active chromospheres produce stronger Ca II K emission). The H line, on the other hand, may be found in various degrees of absorption for low to intermediate levels of activity, and in emission for strong activity. Let us describe a few limiting cases: (1) the majority of the stellar surface is covered with quiet chromosphere and a small fraction of very active regions; (2) the majority of the stellar atmosphere consists of the active component, with a small fraction of the quiet chromosphere, and (3) the majority of the surface is covered in quiet chromosphere and a small fraction of moderately active regions. In the first case, as an active region on the star rotates into view, the equivalent width of Ca II K emission increases, while the H absorption line fills in and also increases in equivalent width (i.e. becomes a shallower and thus "less negative" absorption line). Once this isolated active region rotates out of view, both lines decrease. Our first case would show a positive correlation between Ca II K and H equivalent widths measured over time. In our second case, the majority of the star is producing both Ca II K and H in emission. As a region of quiet chromosphere rotates into view, Ca II K decreases slightly as both the basal and active Ca II K lines are in emission. The observed H line is now a superposition of an absorption line with the chromospheric emission line, causing the equivalent width to decrease. Again, one would observe a positive correlation between Ca II K and H. In our last scenario, the majority of the star is covered by basal chromosphere producing a weak H absorption line and Ca II K emission, and a moderately active region comes into view. If this moderately active region produces a deeper H absorption line, the equivalent width of H will decrease, while the Ca II K emission will be enhanced. In this case, one would observe a negative correlation between Ca II K and H. In between these extremes, variations in active region coverage and distribution across the stellar surface may explain much of the observed behavior between these two chromospheric tracers.

##### 5. COMPARISON TO UV AND X-RAY DATA

In order to investigate the relationship between the chromosphere and the corona, we compare our optical measurements to archival near-UV and X-ray data. Of the 81 stars observed, 30 have archival X-ray measurements, and a subset of 7 of these stars have near UV (Mg II) measurements. All UV measurements come from active stars (those with H in emission), while the X-ray subsample also includes some moderate and weak activity stars (which have H in absorption). In Table 5, we provide previously published Mg II and X-ray measurements (Wolkowicz et al. 2008; Bookbinder 1985; Johnson 1986; Athioudakis & Doyle 1989, 1992) where available.

Figure 12 plots the X-ray flux versus the Mg II flux for this subsample. Both the X-ray and UV observations were drawn from various sources: X-ray values were taken either from ROSAT observations of nearby stars (Huensch 1999) or EINSTEIN/EXO SAT values origi-

nally reported in Athioudakis & Doyle (1989), noted in the plot legends as "MD89". Measurements of the Mg II flux were taken from either IUE observations (Athioudakis & Doyle 1989) or ACS observations (Wolkowicz et al. 2008). As some of the stars in this subsample have been observed by multiple instruments, the points in each plot are color coded by where the observations originate, and multiple observations of a single object are connected by solid lines between points. Although a number of M dwarfs have been observed with newer X-ray instruments (such as XMM and Chandra) and with higher resolution in the UV (as with STIS or GHRs), our sample is comprised only of M3 dwarfs. We include the ROSAT and Athioudakis & Doyle (1989) data sets because they are available for a number of stars in our sample, not just a select few of the most active ones (e.g., AD Leo and EV Lac). The solid line located to the right is the approximate power law fit to the Mg II and soft X-ray emission in G and K dwarfs reported in Ayres et al. (1981), while the dashed line represents equality between the Mg II and X-ray emission. Our sample seems to obey a similar power law relation as that found by Ayres et al. (1981) for earlier type dwarfs.

Our X-ray and Mg II detected subsample can also be compared to the H and Ca II K measurements reported here, as shown in Figures 13 and 14, respectively. In the plots comparing the flux in the H line, filled points indicate H in emission and unfilled points indicate H in absorption. The Ca II K line always appears in emission.

Figure 14 shows archival UV measurements of Mg II versus our measurements of H and Ca II K. As the Mg II observations are all of relatively active M dwarfs, this figure shows a positive correlation between Mg II and both H and Ca II K, reminiscent of the relationship between H and Ca II K in active stars shown in Figures 4a and 5a.

Figure 13 shows a clear correlation between the optical chromospheric emission and the coronal X-ray emission. The relationship between the coronal emission and the H emission has somewhat less scatter than that between the X-ray and Ca II K flux (the three points that sit to the left of the main locus in Figure 13a, which appear to have anomalously low H flux, are probably intermediate activity stars whose H lines are almost completely filled in with chromospheric emission). The relationship between H and X-rays may be indicative of the link between emission from the upper chromosphere (where H is formed) and the coronal emission. Figures 12 and 13 show that the Ca II K, H and Mg II chromospheric lines trace the coronal X-ray emission in the same way as one another, likely due to this subsample being comprised of active stars, whose greater activity leads to more emission in all lines.

Plasma temperature distributions have been calculated using Chandra data for only two of the most active stars in our sample, AD Leo and EV Lac; the bulk of the plasma lies between  $2 - 20 \times 10^6$  K, peaking around  $7 - 8 \times 10^6$  K for both stars (Robrade & Schmitt 2005). However, ROSAT hardness ratios, which compare the flux in the 'soft' (0.14 - 0.42 keV; S') and 'hard' (0.52 - 2.01 keV; H') bands, are available for a larger number of stars. The hardness ratio,  $(H - S)/(H + S)$ , can be used as a rough proxy for coronal temperature, where harder emission (larger hardness ratio) corresponds to hotter

coronal plasma. Figure 15 shows the hardness ratio for ROSAT detected stars versus the flux in Ca II K and H . It is evident from both of these plots that the chromospheric emission, as traced by H , is positively correlated with the hardness of the coronal emission, albeit with large scatter. In the case of Figure 15b, the two points that appear to have low values of H flux for their coronal hardness are again the intermediate activity stars, where the equivalent width of the line is very small due to its being mostly filled in with emission. The Ca II K chromospheric emission also appears to be loosely correlated with the hardness of the coronal emission, but with far greater ambiguity than seen in the case of H .

We can further examine the relationship between the coronal and chromospheric emission by looking at the ratio of the luminosity in H to the X-ray luminosity versus the hardness ratio. In Figure 16, unfilled symbols indicate H in absorption, while filled symbols indicate H in emission. The two points that lie below this locus are the same two stars with very small H fluxes due to the line being completely filled by chromospheric emission. The median value for the sample as a whole is  $\log(L_H/L_X) = 0.6$ , which is consistent with the values reported by Reid, Hawley & Mateso (1995) for low mass stars in the Hyades ( $\log(L_H/L_X) = 0.6$ ) and Pleiades ( $\log(L_H/L_X) = 0.8$ ). For the most part, there is no obvious trend in the data (however for the most active stars, there appears to be a slight indication that the X-ray luminosity increases proportionately with the coronal temperature, shown here as a slight negative correlation in the filled data points. Considering the dM and dMe stars separately, the median value of  $\log(L_H/L_X)$  for the dM stars is  $\log(L_H/L_X) = 0.45$ , somewhat higher than the dMe sample, where  $\log(L_H/L_X) = 0.84$ . These results are also consistent with those reported in Skumanich et al. (1984) and Fleming (1988) for field M dwarfs.

Figure 16 also compares the ratio of the chromospheric to coronal emission, respectively measured by H and X-rays, to model predictions of the minimum X-ray flux in late type stars. The colored bars in this plot correspond to our measured H flux divided by the range of X-ray flux generated by various models of coronal heating: model predictions of acoustically heated coronae ( $\log F_X = 5.1 \text{ ergs s}^{-1} \text{ cm}^{-2}$ ; Mullan & Cheng 1994), and the X-ray flux predicted by models of magnetic field generation in the convective envelopes of non-rotating stars ( $\log F_X = 3.8 \text{ ergs s}^{-1} \text{ cm}^{-2}$ ; Bercik et al. 2005). Red bars indicate stars with H in emission, while blue bars indicate stars with H in absorption. Points lying below their accompanying bars exceed the amount of coronal emission that can be explained by either of these models, while the X-ray flux of points lying within their colored bars could potentially be explained by either prediction. All of the active stars (dMe; filled diamonds) exceed the level of coronal emission produced in purely acoustic models, in accordance with the role global, rotationally dependent magnetic activity is believed to play in the heating of the outer atmospheres of these stars. In the case of the dM stars (open diamonds), the behavior is more complicated (in most cases the coronal flux exceeds both predictions, but in some cases it does not. This observation may provide another indication that two components are at work in the outer atmospheres of M dwarfs (hot, active regions associated with global magnetic activ-

ity, coexisting with cooler basal regions that may be associated with small scale convectively-generated magnetic fields, analogous to quiet regions on the Sun. The relative filling factors of these two components may explain much of the variation we see in M dwarf chromospheric and coronal emission.

## 6. CONCLUSIONS AND FUTURE WORK

The observations presented in this paper provide a rich set of empirical constraints for the construction of new model chromospheres. We find that for weak to intermediate activity stars, there is a range in the equivalent width of Ca II K emission for a small range of H absorption. Our high resolution data indicate that the H line may undergo an initial increase in absorption, as Ca II K increases, with the line filling in and eventually going into emission for the most active stars as observed by Staufer & Hartmann (1986) and predicted by Cram & Giampana (1987). From H observations alone, it is impossible to distinguish between a moderately active and an inactive star. Therefore, studies of activity in low mass stars that focus solely on stars with H in emission are biased towards the most active chromospheres. These active stars have both Ca II and Balmer lines in emission, and more active stars have stronger emission in both lines. This positive correlation between Ca II K and Balmer emission in single observations of active stars does not imply, however, that the chromospheric tracers are positively correlated over time for every star. The variation in chromospheric emission of individual stars is most likely a function of the quiet and active region coverage unique to their particular stellar atmosphere.

That lateral inhomogeneity may play a major role in the observed spectra of our M3 sample is not surprising, given observations of active regions on the Sun, and the inferred large filling factors of active regions deduced from M dwarf magnetic field measurements and observations of ares (e.g. Basri et al. 1990; Johns-Krull & Valenti 1996; O’Neale et al. 2004). In the scenario we propose, stronger chromospheric emission would correspond to a greater presence of active regions on the stellar surface due to the increased influence of the magnetic field. If Ca II K and H are produced preferentially by cool and hot components, respectively, one would expect that while greater chromospheric heating would cause more emission in both lines, the relation between the two lines would be increasingly decoupled as the hotter active component becomes more prominent.

We are in the process of further investigating whether two-component model atmospheres can account for the relationships between the Ca II and the Balmer lines. Using the data described here as empirical constraints, we are developing a new generation of quiescent non-LTE model atmospheres for M dwarfs. These two-component static models will be calculated using the non-LTE radiative transfer program RH described in Uitenbroek (2001). RH allows for bound-bound and bound-free radiative transitions to overlap in wavelength and includes the effects of partial redistribution for strong bound-bound transitions, essential for proper treatment of the Ca II and Balmer lines. This effort complements recent work on modeling the outer atmospheres of M dwarfs during flaring states with the radiative-hydrodynamic non-LTE transfer code RADYN (Carlsson & Stein 1997;



Abbett & Hawley 1999; Allred et al. 2005). These new models will address both the observed line fluxes and correlations between Ca IIR and the Balmer lines obtained from our lower resolution data, and in addition will allow us to compare the detailed model line profiles to our echelle observations for a subset of our sample stars.

LMW thanks Geomarcy and Gabor Basri for providing generous access to the California Planet Search HRES spectra, as well as Chris Johns-Krull and Andrew West for illuminating conversations and assistance in data analysis. LMW and SLH additionally thank Jeff

frey Linsky for his valuable comments as our referee, which have greatly improved this publication. Support for this work, associated with HST program GO-10525, was provided by NASA through a grant from the Space Telescope Science Institute, which is operated by the Association of Universities for Research in Astronomy, Inc., under NASA contract NAS 5-26555. The authors also wish to recognize and acknowledge the very significant cultural role and reverence that the summit of Mauna Kea has always had within the indigenous Hawaiian community.

## REFERENCES

- Abbett, W. P. 2008, *Subsurface and Atmospheric Influences on Solar Activity* ASP Conference Series, 383, 327
- Ayres, T. R., Marstad, N. C., & Linsky, J. L. 1981, *ApJ*, 247, 545
- Basri, G., Valenti, J. A., & Marcy, G. W. 1990, *ApJ*, 360, 650
- Berck, D. J., Fisher, G. H., Johns-Krull, C. M., & Abbett, W. P. 2005, *ApJ*, 631, 529
- Berck, D. J., Fisher, G. H., Johns-Krull, C. M., Abbett, W. P., & Lundquist, L. L. 2006, *Solar MHD Theory and Observations: A High Spatial Resolution Perspective* ASP Conference Series, 354, 127
- Bookbinder, J. A. 1985, Ph.D. Thesis.
- Browning, M. K. 2008, *ApJ*, 676, 1262
- Burgasser, A. J., Kirkpatrick, J. D., Reid, I. N., Liebert, J., Gizis, J. E., & Brown, M. E. 2000, *AJ*, 120, 473
- Butler, R. P., Marcy, G. W., Williams, S. E., McCarthy, C., Osan, J. P., & Vogt, S. S. 1996, *PASP*, 108, 500
- Carpenter, J. M. 2001, *AJ*, 121, 2851
- Chabrier, G., & Baraffe, I. 1997, *A & A*, 327, 1039
- Cincunegui, C., Diaz, R. F., & Maas, P. J. D. 2007, *A & A*, 469, 309
- Cram, L. E., & Mullan, D. J. 1985, *ApJ*, 294, 626
- Cutri, R. M., et al. 2003, *VizieR Online Data Catalog*, 2246, 0
- Cram, L. E., & Giamppa, M. S. 1987, *ApJ*, 323, 316
- Durney, B. R., De Young, D. S., & Roxburgh, I. W. 1993, *Sol. Phys.*, 145, 207
- Fleming, T. A. 1988, *PASP*, 100, 1186
- Foukal, P. 1990, *New York, Wiley-Interscience*, 1990, 492 p.
- Giamppa, M. S., Worden, S. P., & Linsky, J. L. 1982, *ApJ*, 258, 740
- Gizis, J. E., Monet, D. G., Reid, I. N., Kirkpatrick, J. D., Liebert, J., & Williams, R. J. 2000, *AJ*, 120, 1085
- Gizis, J. E., Monet, D. G., Reid, I. N., Kirkpatrick, J. D., & Burgasser, A. J. 2000, *MNRAS*, 311, 385
- Gizis, J. E., Reid, I. N., & Hawley, S. L. 2002, *AJ*, 123, 3356
- Hasan, S. S., & van Ballegoijen, A. A. 2008, *ApJ*, 680, 1542
- Hawley, S. L., Gizis, J. E., & Reid, I. N. 1996, *AJ*, 112, 2799
- Hawley, S. L., & Johns-Krull, C. M. 2003, *ApJ*, 588, L109
- Reid, I. N., & Hawley, S. L. 2005, *New Light on Dark Stars Red Dwarfs, Low-Mass Stars, Brown Stars*, by I. N. Reid and S. L. Hawley. Springer-Praxis books in astrophysics and astronomy. Praxis Publishing Ltd, 2005. ISBN 3-540-25124-3
- Reid, I. N., Gizis, J. E., & Hawley, S. L. 2002, *AJ*, 124, 2721
- Reid, I. N., et al. 2004, *AJ*, 128, 463
- Robinson, R. D., Cram, L. E., & Giamppa, M. S. 1990, *ApJS*, 74, 891
- Robrade, J., & Schmitt, J. H. M. M. 2005, *A & A*, 435, 1073
- Rutten, R. G. M. 1987, *A & A*, 177, 131
- Rutten, R. J. 2006, *Solar MHD Theory and Observations: A High Spatial Resolution Perspective*, 354, 276
- Rutten, R. J. 2007, *The Physics of Chromospheric Plasmas*, 368, 27
- Schrijver, C. J., Dobson, A. K., & Radick, R. R. 1989, *ApJ*, 341, 1035
- Schrijver, C. J. 1988, *A & A*, 189, 163
- Skumanich, A., Young, A., Stauder, J., & Bopp, B. W. 1984, *BAAAS*, 16, 940
- Stauder, J. R., & Hartmann, L. W. 1986, *INP Vol. 254: Cool Stars, Stellar Systems and the Sun*, 254, 58
- Sundland, S. R., Pettersen, B. R., Hawley, S. L., Kjeldseth-Moe, O., & Andersen, B. N. 1988, *Activity in cool star envelopes*, p. 61–64, 61
- Uitenbroek, H. 2001, *ApJ*, 557, 389
- Vogler, A., & Schussler, M. 2007, *A & A*, 465, L43
- Vogt, S. S., et al. 1994, *Proc. SPIE*, 2198, 362
- Walkowicz, L. M., Johns-Krull, C. M., & Hawley, S. L. 2007, accepted to *ApJ*, arXiv:0711.1861
- Walkowicz, L. M., et al. in prep.
- West, A. A., et al. 2004, *AJ*, 128, 426
- West, A. A., et al. 2006, *Bulletin of the American Astronomical Society*, 38, 1024
- West, A. A., Hawley, S. L., Bochanski, J. J., Covey, K. R., Reid, I. N., Dhital, S., Hilton, E. J., & Masuda, M. 2008, *AJ*, 135, 785
- West, A. A., in prep.

W right, J. T ., M arcy, G . W ., Butler, R . P ., & Vogt, S . S . 2004,  
ApJS, 152, 261  
Young, A ., Skum anich, A ., & Harlan, E . 1984, ApJ, 282, 683

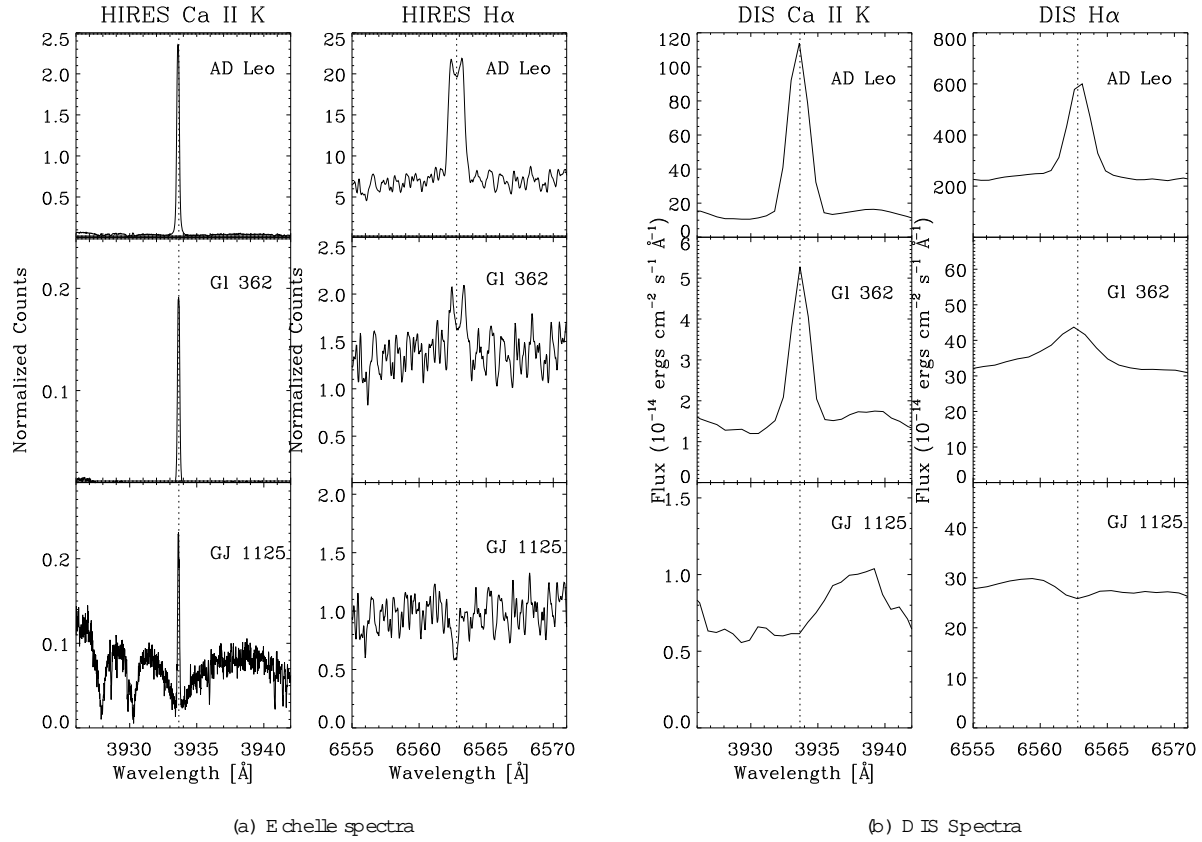


Fig. 1. | Example H IRES (left) and D I S (right) observations of Ca II K and H  $\alpha$  for three stars of varying activity level. Top: AD Leo, high activity; M iddle: G I 362, m oderate activity; B ottom : G J 1125, low activity. It is evident that even stars that appear to be inactive at low resolution (e.g. G J 1125) may still show chrom ospheric Ca II K emission in high resolution spectra.

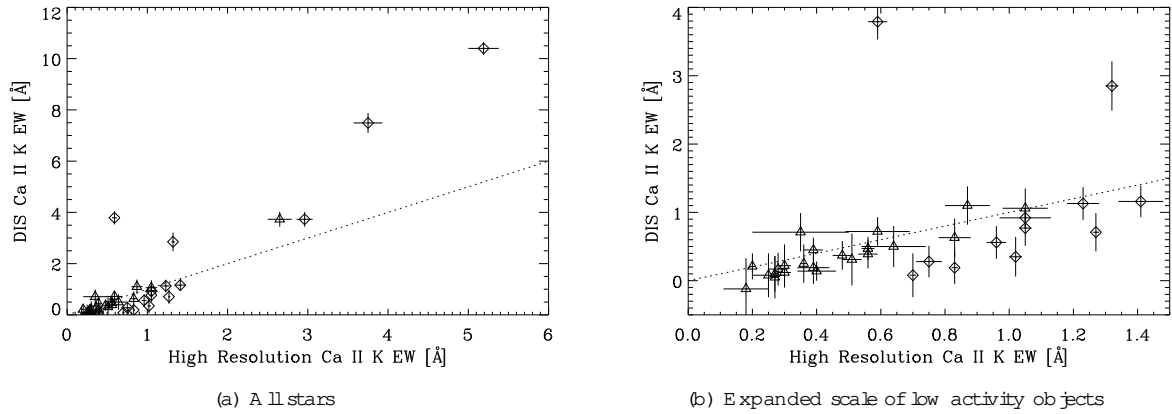


Fig. 2. | Comparison between Ca II K equivalent widths measured from low resolution data corrected for the photospheric contribution, and equivalent widths measured by fitting the Ca II K emission core in high resolution data. Diamonds denote measurements of our ARCES echelle data, while triangles indicate measurements from H IRES echelle data. The dotted line represents the locus of agreement for the two equivalent width measurements. For small equivalent width, the two methods of measurement produce comparable results, and the points lie along the line of agreement. However, for the most active the equivalent widths measured from the low resolution data are larger than those measured from the high resolution data. This difference is due to how the photospheric absorption line is accounted for in our two measurement methods: the method used for measuring the high resolution data underestimates the chrom ospheric contribution to the line. The two points in (b) which lie significantly above the locus are two stars that were observed with D I S during higher activity states than their echelle observations.

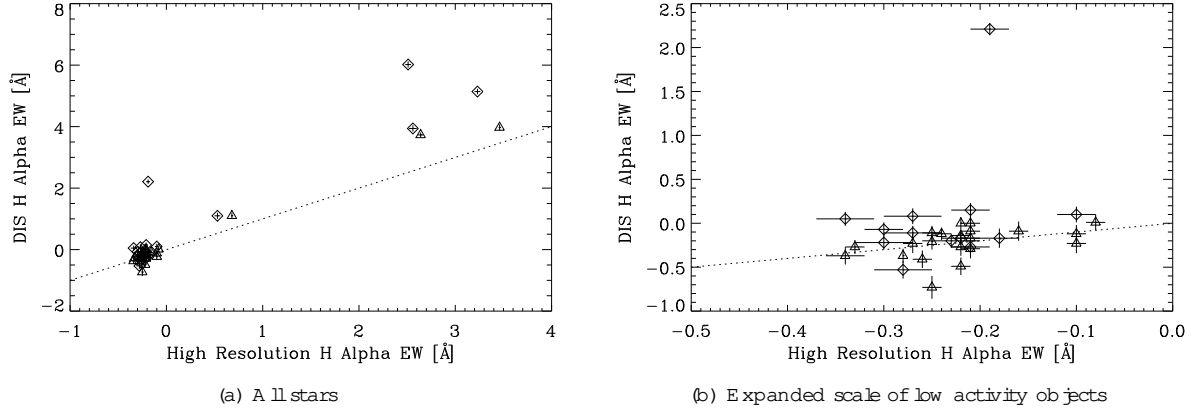


Fig. 3. Comparison between H  $\alpha$  equivalent widths calculated from DIS and echelle spectra. The dotted line represents the locus of agreement for the two equivalent width measurements. Diamonds denote measurements of our ARCES echelle data, while triangles indicate measurements of HRES echelle data. As in the case of the Ca II K line, the two methods of measurement produce comparable results for small equivalent widths. However, for the most active the equivalent widths measured from the low resolution data are larger than those measured from the high resolution data. This discrepancy is caused by the H  $\alpha$  line falling close to the edge of the order in our echelle spectra (the continua in our echelle spectra have a different slope than the low resolution spectra, which causes the continuum value, and thus the equivalent width, to be underestimated in the echelle measurements). The point in (b) which lies significantly above the locus is a star observed with DIS during a higher activity state than its echelle observation.

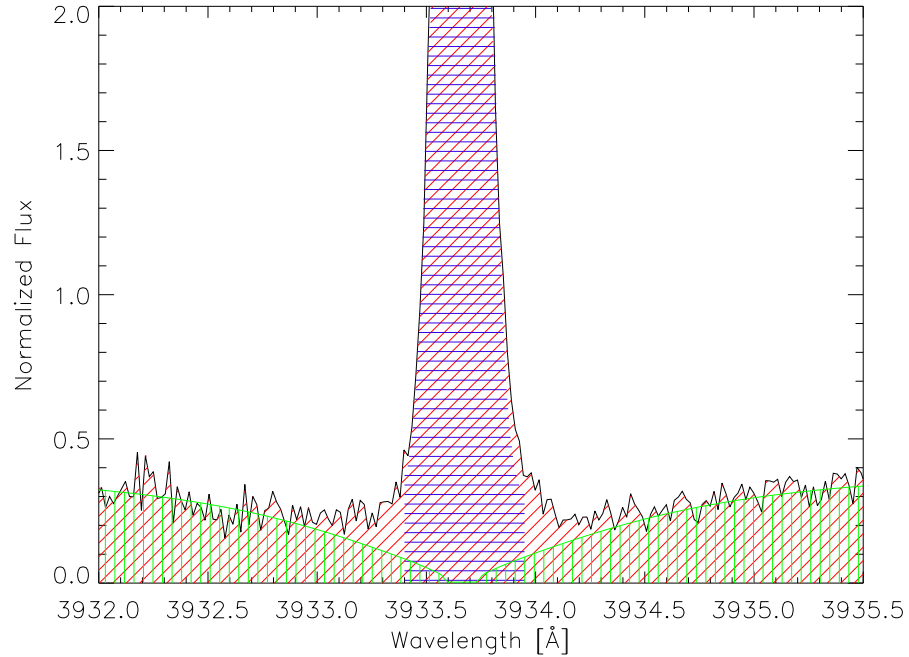


Fig. 4. The total flux in Ca II K (red diagonal hatching) is comprised of a chromospheric emission core (blue horizontal hatching) superimposed over a photospheric absorption line (green vertical hatching). However, some flux in the inner line wings is also chromospheric, i.e. the flux exceeds that predicted by the radiative equilibrium model absorption line (green vertical hatching). Our method of measuring the Ca II K line corrects for the photospheric contribution to the line by subtracting off the radiative equilibrium profile, thereby measuring only the chromospheric flux in Ca II K.

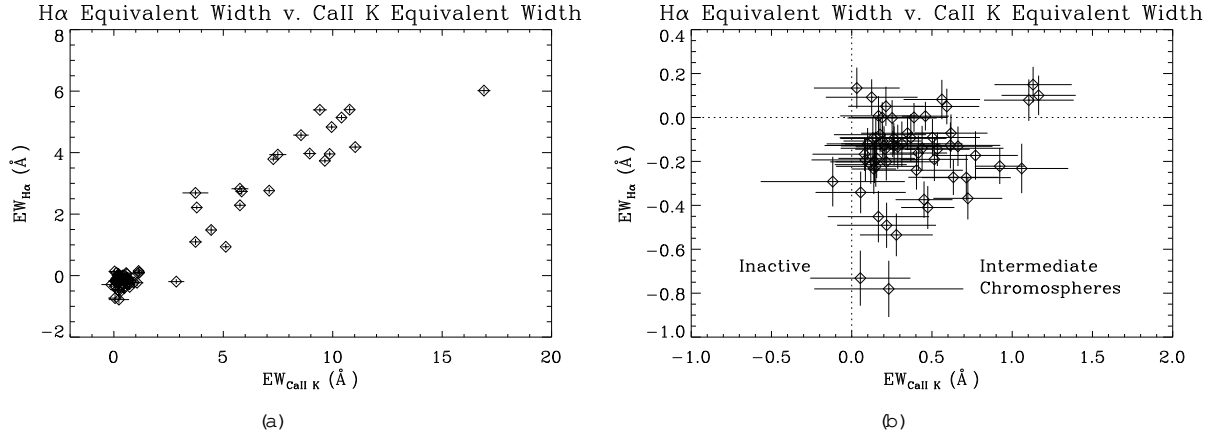


Fig. 5. (a): Total  $H\alpha$  equivalent width versus chromospheric Ca II K for the entire sample observed with DIS. For low to intermediate activity objects (those with  $H\alpha$  absorption) there is no obvious correlation with Ca II K. However, active stars show a positive correlation between the lines. (b): Total  $H\alpha$  equivalent width versus chromospheric Ca II K, shown at an expanded scale for the weak to intermediate activity stars. The perpendicular dotted lines plotted over the data indicate zero  $H\alpha$  and Ca II K equivalent widths (stars with  $H\alpha$  absorption (negative equivalent width) would traditionally be classified as "inactive", but many of these stars possess small chromospheric Ca II K emission). Increasing absorption in  $H\alpha$  as Ca II K increases is not evident from these low resolution data.

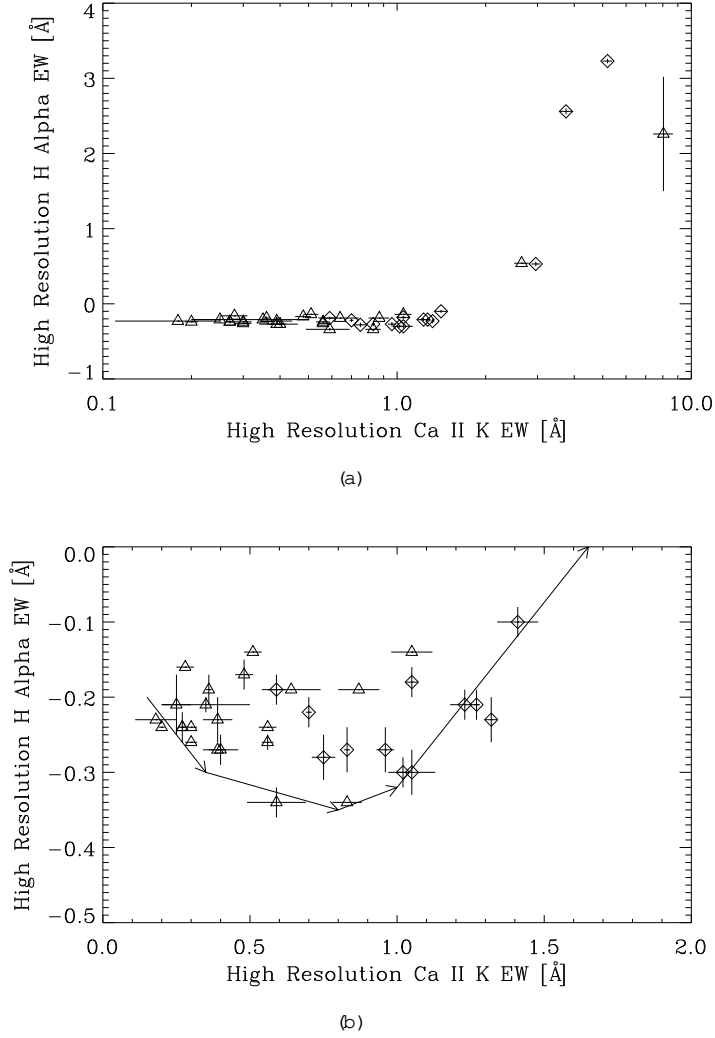


Fig. 6. (a:) H and Ca II K equivalent widths measured from our echelle spectra. Diamonds denote measurements of our ARCES echelle data, while triangles indicate measurements from our HRES data. As in the case of the low resolution observations, H absorption is associated with a range in Ca II K emission, while H emission seems to be positively correlated with Ca II K. The weak to intermediate activity objects, plotted at an expanded scale in (b), seem to indicate an initial increase in H absorption with increasing Ca II K, as per the observations of Staufer & Hartmann (1986). The arrows indicate the schematic locus (predicted by Cram & Giampa 1987) of an initial increase in H absorption as Ca II K increases, and subsequent falling in with emission as Ca II K increases even further. Interestingly, the locus appears to delineate the envelope of the observations.

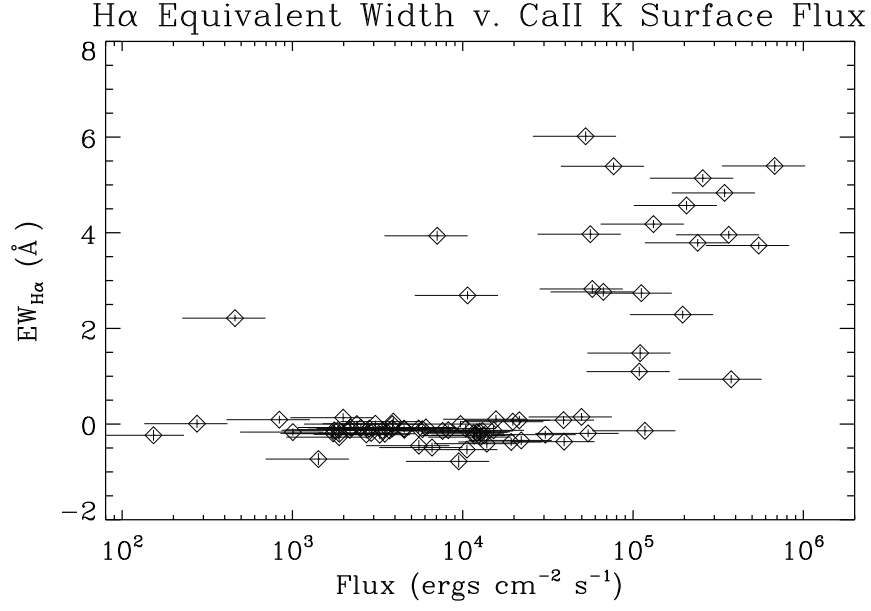


Fig. 7. |  $H\alpha$  equivalent width versus the Ca II K surface flux measured from our low resolution DIS data. More active stars (those with larger Ca II K flux) have a wide range of scatter in their  $H\alpha$  equivalent widths.

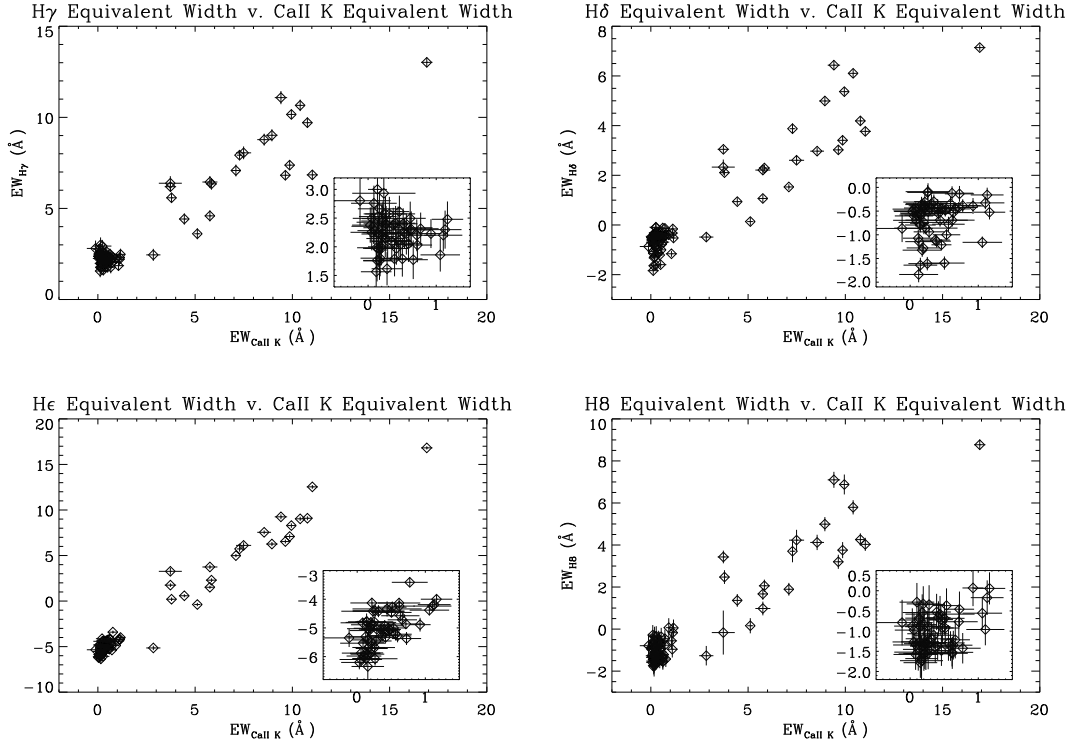


Fig. 8. | Equivalent widths for higher order Balmer lines versus Ca II K equivalent widths from DIS data. The higher order line and Ca II K show a similar relationship as Ca II K did with  $H\alpha$  in Figure 4(a).

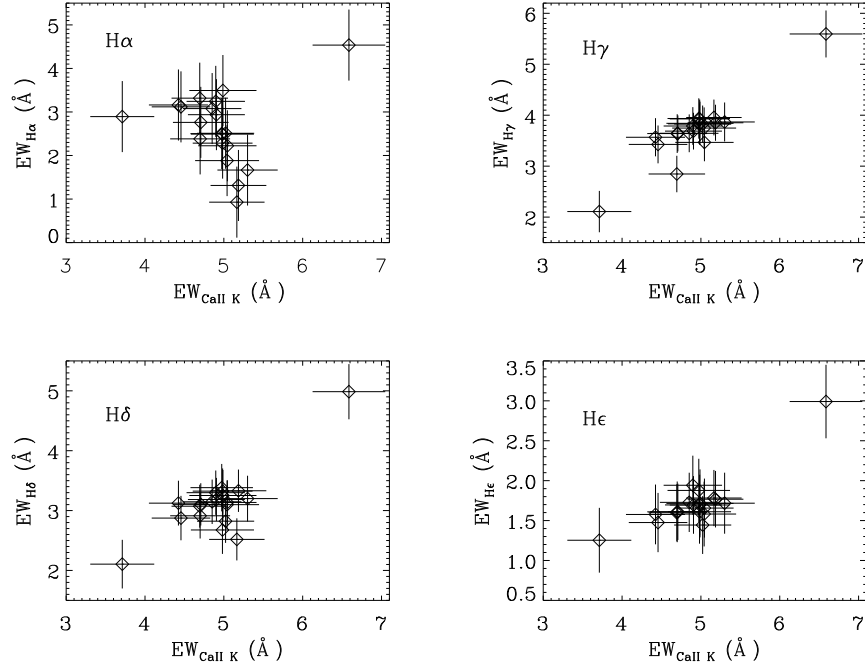


Fig. 9. | Multiple measurements of equivalent widths of the Balmer lines and Ca II K in the active star AD Leo, measured from HIRES echelle data. Although a positive correlation between the instantaneous measurements of H $\alpha$  and Ca II K is evident in Figures 2 and 3, it is clear that the two lines are not necessarily positively correlated in time-resolved observations of a single star.

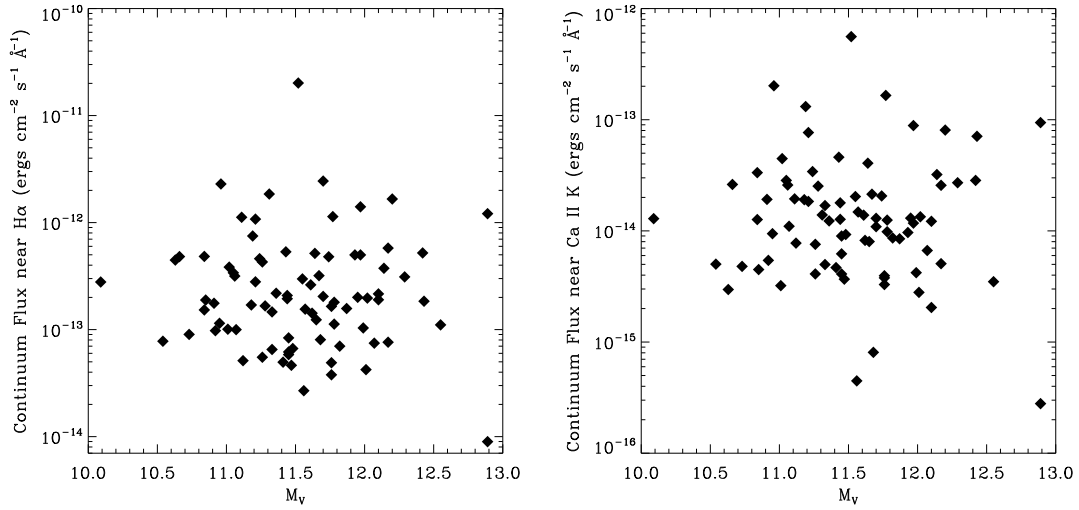


Fig. 10. | Continua near H $\alpha$  and Ca II K from our flux-calibrated DIS data versus absolute V magnitude. There is no discernable trend between the continuum level and the absolute magnitude of the stars in our sample.



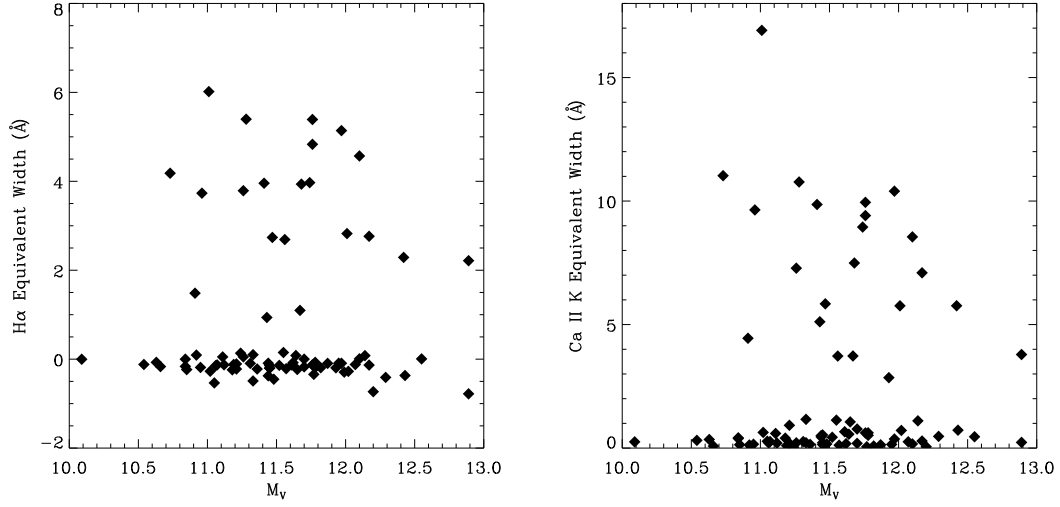


Fig. 11. Equivalent widths of H  $\alpha$  and Ca II K (measured from DIS data) versus absolute V magnitude. The activity levels we determine for each star show no bias towards higher luminosity stars.

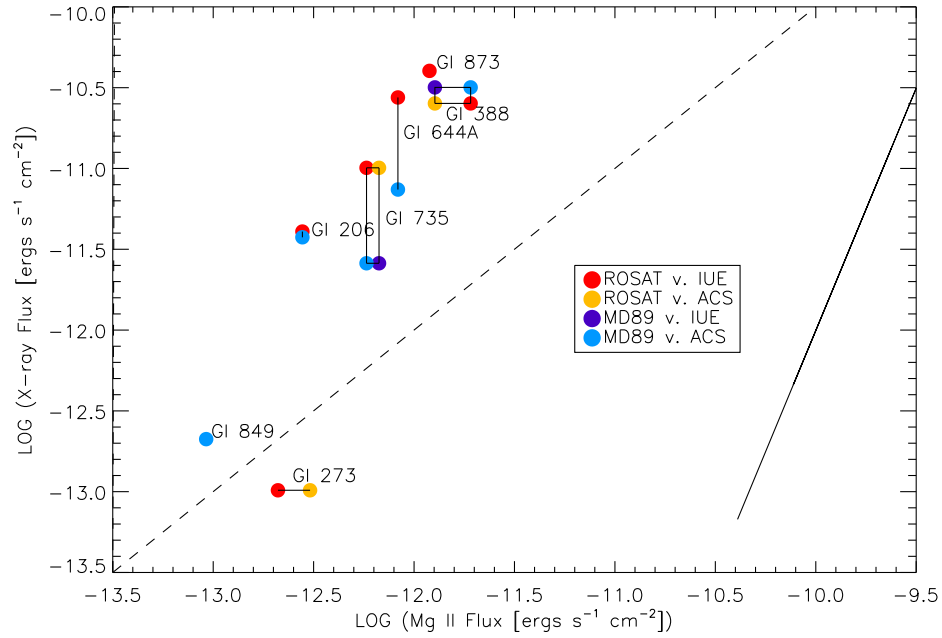


Fig. 12. X-ray flux versus Mg II flux for a subset of our sample. Different plotting symbols are used to indicate measurements by different instruments. Points corresponding to multiple observations of a given star by different instruments are connected by solid lines. The solid line at right represents the approximate power law fit to Mg II and soft X-ray emission of G and K dwarfs given in Ayres et al. (1981), while the dashed line indicates the line of equality between the Mg II and X-ray emission.

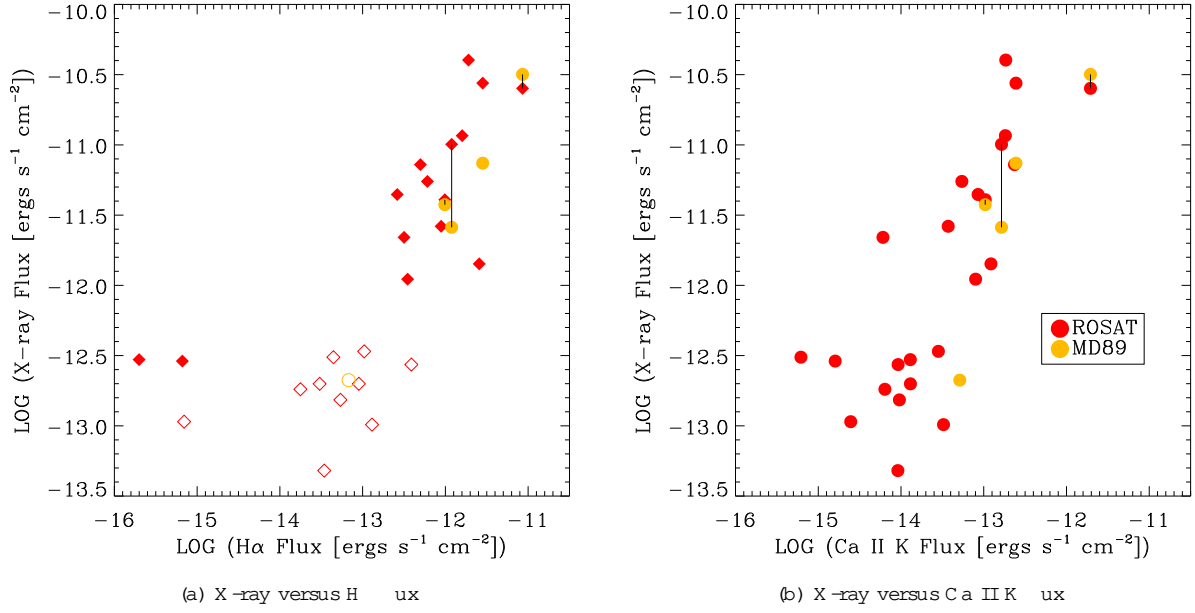


Fig. 13. | X-ray flux versus the optical chromospheric flux as measured by H $\alpha$  and Ca II K (measured from flux-calibrated DIS data). In (a), open circles correspond to H $\alpha$  absorption, while filled circles denote H $\alpha$  emission. As the Ca II K line flux we report is always due to the chromospheric emission core, all symbols in (b) are filled to indicate emission. The three points that lie to the left of the main locus in (a) are H $\alpha$  lines with very low equivalent width, probably due to their being almost completely filled in by chromospheric emission.

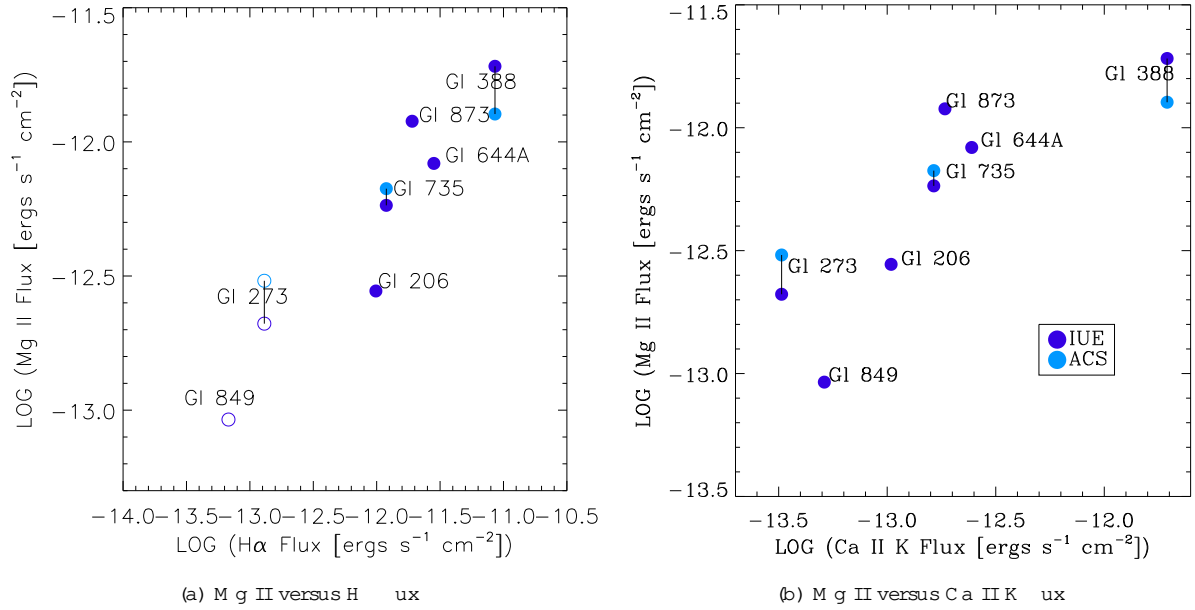
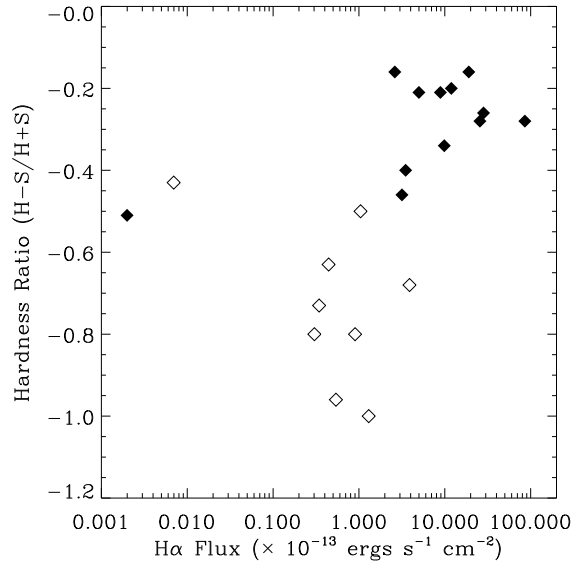
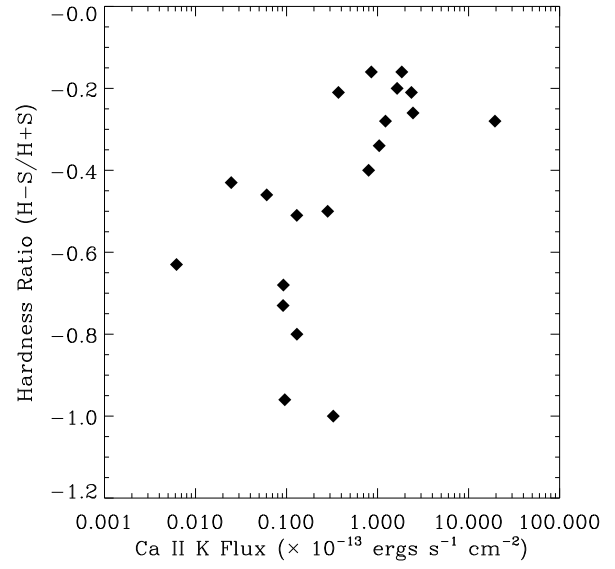


Fig. 14. | UV chromospheric (Mg II) flux versus the optical chromospheric flux as measured by H $\alpha$  and Ca II K. Different plotting symbols indicate Mg II measurements taken with either IUE or the ACS near-UV prism; multiple observations of stars are connected with solid lines. In (a), two of the stars with Mg II measurements have H $\alpha$  absorption (these are indicated by open plotting symbols, while emission is denoted by filled symbols). In the Mg II sample of active stars, the positive correlation is reminiscent of that for Ca II K and H $\alpha$  in our optical measurements.



(a) Hardness ratio versus  $H$



(b) Hardness ratio versus Ca II K

Fig. 15. Hardness ratio versus measurements of  $H$  and Ca II K flux from DIS data. Open diamonds in (a) denote  $H$  absorption, while filled diamonds indicate emission. Increasing hardness is indicative of hotter coronal temperatures, and correlates with increasing flux in the chromospheric lines.

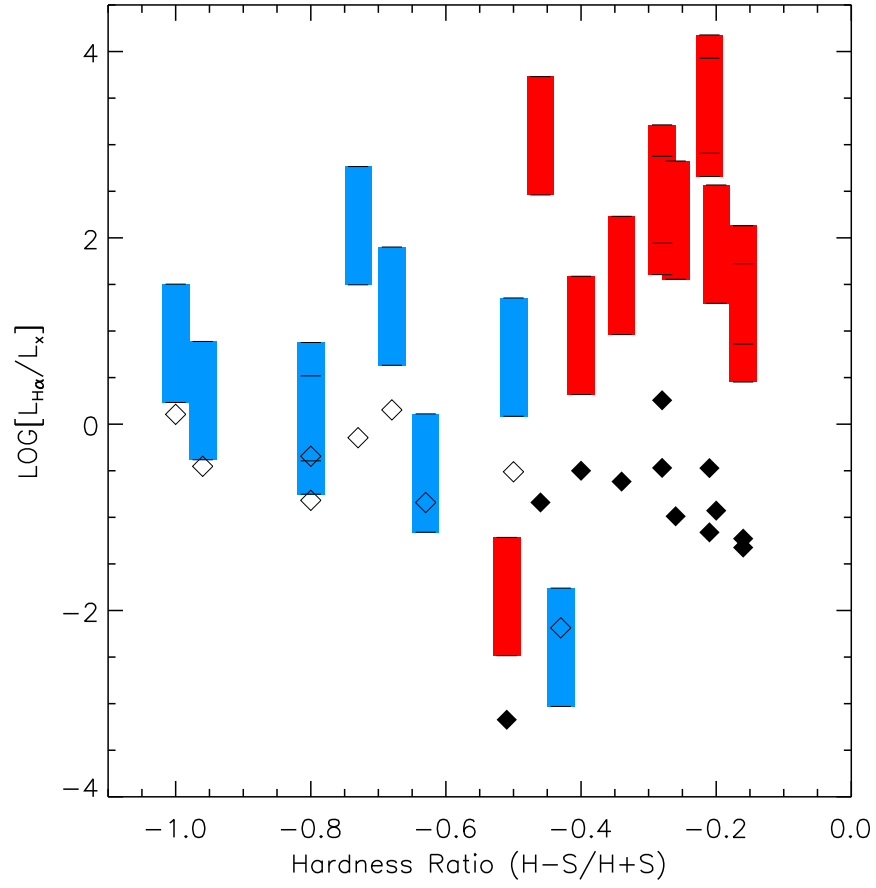


Fig. 16. Ratio of the luminosity in  $H\alpha$  to the X-ray luminosity versus the hardness ratio. Open diamonds indicate  $H\alpha$  absorption, while filled symbols indicate  $H\alpha$  emission. Stars lie at a roughly constant value of  $L_{H\alpha}/L_x \approx -0.6$ , consistent with observations of both field and cluster M dwarfs.

TABLE 1  
Summary of Program Stars

CNS3	Name	2000	2000	$M_V$	d (pc)	SpT
460	G J 3168	02 36 27.2	+ 55 28 35	11.45	22.6	M 3
492	G 1109	02 44 14.9	+ 25 31 25	11.07	8	M 3
836	G 1179	04 52 05.6	+ 06 28 37	11.65	11.6	M 3.5
876	G J 3333	05 07 49.2	+ 17 58 59	11.24	12.8	M 3
919	G 1203	05 28 00.1	+ 09 38 43	12.42	10.3	M 3.5
933	G 1206	05 32 14.6	+ 09 49 15	10.95	13	M 3.5
941	G J 3356	05 34 52.1	+ 13 52 48	11.44	11.8	M 3.5
1068	G J 3404A	06 42 11.1	+ 03 34 54	11.62	12.2	M 3.5
1089	G J 3412	06 54 03.7	+ 60 52 24	10.91	10.7	M 3
1094	G 1251	06 54 49.4	+ 33 16 07	11.21	5.8	M 3
1126	G 1263	07 04 17.2	10 30 08	10.63	13.5	M 3.5
1168	G 1273	07 27 30.8	+ 05 13 12	11.97	3.8	M 3.5
1184	G 1277B	07 31 57.4	+ 36 13 48	11.43	11.7	M 3.5
1226	G J 1101	07 55 55.5	+ 83 23 08	12.55	12.8	M 3.5
1247	G J 1105	07 58 12.5	+ 41 18 19	12.43	8.2	M 3.5
1328	G J 2069A	08 31 37.6	+ 19 23 39	12.1	9.1	M 3.5
1353	G J 3511B	08 39 48.2	+ 08 56 16	12.07	15.1	M 3.5
1405	G J 3522	08 58 56.1	+ 08 28 28	12.17	5.6	M 3.5
1420	G J 3527	09 01 10.7	+ 01 56 35	11.36	12.3	M 3
1441	G J 3537	09 09 39.2	+ 06 42 08	11.26	26.2	M 3
1501	G J 1125	09 30 44.8	+ 00 19 25	11.68	10.1	M 3.5
1507	G 1352A	09 31 18.9	13 29 18	11.01	9.1	M 3
1530	G 1363	09 42 23.8	+ 55 59 05	11.78	14	M 3.5
1529	G 1362	09 42 52.5	+ 70 02 23	11.05	10.8	M 3
1611	G 1386	10 16 46.1	11 57 36	10.92	10.3	M 3
1616	G 1388	10 19 36.4	+ 19 52 11	10.96	4.9	M 3
1657	G J 361	10 35 29.0	+ 69 27 03	11.45	12.5	M 3.5
1658	G 1398	10 36 01.5	+ 05 07 10	11.97	13.4	M 3.5
1660	G J 3613	10 38 27.4	+ 48 32 05	11.41	26	M 3
1690	G 1403	10 52 04.6	+ 13 59 48	12.1	13	M 3.5
1742	G J 3647	11 11 51.8	+ 33 32 09	11.76	13.3	M 3.5
1795	G J 3666	11 28 56.5	+ 10 10 34	11.77	14.4	M 3.5
1838	G 1443	11 46 42.5	14 00 43	11.21	12.4	M 3
1845	G 1445	11 47 39.2	+ 78 41 24	12.2	5.3	M 3.5
1931	G J 3719	12 16 58.5	+ 31 09 22	11.76	30	M 3.5
1988	G 1480	12 38 53.1	+ 11 41 47	11.11	12.1	M 3
2009	G 1486	12 47 57.2	+ 09 45 09	11.78	8.3	M 3.5
2088	G J 3775	13 18 01.9	+ 02 14 00	11.76	17.4	M 3.5
2094	G 1507B	13 19 34.4	+ 35 06 30	11.45	13.5	M 3
2175	G J 3804	13 45 50.9	17 57 56	11.67	10.9	M 3.5
2300	G 1553.1	14 31 01.4	12 17 43	11.7	11.1	M 3.5
2399	G J 3892	15 09 35.9	+ 03 09 56	11.18	11.4	M 3
2420	G 1581	15 19 27.5	07 43 20	11.52	6.4	M 3
2456	G J 3913	15 35 46.5	+ 22 09 46	11.48	17.5	M 3.5
2472	G 1597	15 41 14.7	+ 75 59 38	11.55	13.6	M 3
2567	G 1617B	16 16 45.8	+ 67 15 20	10.54	10.9	M 3
2587	G J 3953	16 25 32.4	+ 26 01 37	11.33	15.2	M 3
2599	G 1628	16 30 18.0	12 39 35	12.02	4.1	M 3.5
2660	G 1643	16 55 24.6	08 19 27	12.89	6.1	M 3.5
2660	G 1643	16 55 24.6	08 19 27	12.89	6.1	M 3.5
2661	G 1644A	16 55 28.1	08 20 16	10.66	6.4	M 3
2665	G J 1207	16 57 05.4	04 20 52	12.29	10	M 3.5
2700	G 1655	17 07 07.6	+ 21 33 14	10.84	14.3	M 3
2714	G J 3992	17 11 34.5	+ 38 26 33	11.7	9.6	M 3.5
2712	G 1660A	17 11 52.4	01 51 02	11.64	12.1	M 3
2717	G 1661A	17 12 07.5	+ 45 40 09	11.02	6.1	M 3.5
2719	G J 1212	17 13 40.6	08 25 11	11.26	14.4	M 3.5
2744	G 1669A	17 19 54.5	+ 26 30 01	11.31	10.5	M 3.5
2797	G 1687	17 36 26.3	+ 68 20 30	10.85	4.6	M 3
2846	G J 4038	17 57 03.6	+ 15 46 45	11.44	14.3	M 3
2851	G J 4040	17 57 50.9	+ 46 35 14	11.12	13.6	M 3
2888	G J 4048	18 18 04.1	+ 38 46 40	11.57	11.5	M 3
2895	G J 1226	18 20 57.4	01 02 48	11.87	14.7	M 3.5
2898	G 1712	18 22 07.3	+ 06 20 36	11.82	14.2	M 3.5
2901	G J 4055	18 23 28.3	+ 28 10 05	11.93	13	M 3.5
2916	G J 4062	18 31 58.4	+ 40 41 06	11.61	11.9	M 3.5
2921	G J 4063	18 34 36.5	+ 40 07 27	12.14	7.2	M 3.5
2924	G 1720B	18 35 26.9	+ 45 45 38	12.17	14.8	M 3.5
2937	G J 4068	18 35 51.8	+ 80 05 37	12.01	17.5	M 3.5
2940	G J 4070	18 41 59.1	+ 31 49 49	11.06	11	M 3
2945	G 1725A	18 42 48.0	+ 59 37 29	11.19	3.5	M 3
2946	G 1725B	18 42 48.0	+ 59 37 29	11.99	3.5	M 3.5
2964	G J 4083	18 50 45.0	+ 47 58 19	11.95	13	M 3.5
2976	G 1735	18 55 27.3	+ 08 24 09	10.09	10.1	M 3
3013	G J 4098	19 08 29.9	+ 32 16 53	11.33	12.4	M 3
3032	G J 9652A	19 14 39.5	+ 19 18 59	10.73	14.6	M 3.5
3058	G J 4110	19 26 49.3	+ 16 43 03	11.47	21.1	M 3
3306	G J 9721B	21 08 44.8	04 25 17	11.56	23.4	M 3
3425	G J 4231	21 52 10.3	+ 05 37 35	11.28	14.6	M 3
2478	G 1849	22 09 45.2	04 28 11	10.84	8.1	M 3.5

TABLE 2  
Wavelength Regions Used in Line Calculations

Line	Blue Continuum (Å)		Line (Å)		Red Continuum (Å)	
H 8	3850.00	3880.00	3884.15	3898.15	3910.00	3930.00
Ca II K	3952.80	3956.00	variable <sup>a</sup>		3974.80	3976.00
H	4060.00	4080.00	4097.00	4110.00	4120.00	4140.00
H	4270.00	4320.00	4331.69	4350.00	4360.00	4410.00
H	6500.00	6550.00	6557.61	6571.61	6575.00	6625.00

<sup>a</sup>Integration region for the Ca II K line was chosen interactively for individual spectra.

TABLE 3  
Equivalent Widths Measured from DIS Data

[RHG 95]	Name	Ca II K (Å)	κ (Å)	H (Å)	H (Å)	H 8 (Å)	H 8 (Å)	H (Å)	H (Å)	H (Å)	H (Å)	H (Å)	H (Å)
460	G J 3168	0.53	0.20	5.00	0.18	0.37	0.43	1.00	0.27	2.24	0.12	0.14	0.08
492	G 1109	0.39	0.21	5.06	0.19	0.53	0.45	1.13	0.30	1.79	0.14	0.00	0.07
836	G 1179	1.06	0.29	4.38	0.18	0.56	0.41	1.16	0.29	1.86	0.12	0.23	0.11
876	G J 3333	0.46	0.15	5.01	0.15	1.48	0.38	1.21	0.28	2.61	0.11	0.01	0.07
919	G 1203	0.12	0.29	5.30	0.24	0.72	0.41	1.84	0.34	1.98	0.16	0.09	0.08
933	G 1206	8.55	0.36	7.55	0.21	4.12	0.36	2.97	0.33	8.78	0.14	4.57	0.10
941	G J 3356	0.50	0.30	4.46	0.16	0.68	0.41	1.60	0.31	1.79	0.14	0.09	0.08
1068	G J 3404A	0.18	0.29	5.09	0.21	0.54	0.45	1.32	0.32	1.80	0.14	0.08	0.08
1089	G J 3412	0.28	0.23	5.46	0.20	0.34	0.48	0.94	0.29	1.62	0.13	0.53	0.10
1094	G 1251	0.19	0.24	5.01	0.19	0.33	0.44	1.28	0.29	1.97	0.13	0.11	0.08
1126	G 1263	0.35	0.29	5.05	0.22	1.10	0.47	0.30	0.32	2.09	0.15	0.07	0.08
1168	G 1273	0.37	0.21	5.27	0.17	1.40	0.38	1.11	0.30	2.38	0.12	0.09	0.11
1184	G 1277B	5.11	0.16	0.38	0.19	0.16	0.36	0.14	0.30	3.61	0.16	0.94	0.09
1247	G J 1105	0.62	0.23	4.24	0.17	1.55	0.39	0.69	0.29	2.50	0.13	0.07	0.09
1328	G J 2069A	16.91	0.29	16.82	0.18	8.77	0.25	7.14	0.27	13.02	0.13	6.02	0.10
1353	G J 3511B	0.26	0.30	5.68	0.28	1.06	0.56	0.11	0.30	2.57	0.16	0.12	0.06
1405	G J 3522	7.10	0.21	4.99	0.17	1.90	0.30	1.53	0.33	7.08	0.11	2.76	0.10
1420	G J 3527	0.15	0.25	5.91	0.17	1.78	0.38	1.64	0.33	2.22	0.16	0.22	0.09
1441	G J 3537	7.28	0.15	5.73	0.30	3.70	0.53	3.88	0.28	7.92	0.21	3.79	0.08
1501	G J 1125	0.25	0.28	4.79	0.17	1.31	0.40	1.61	0.32	2.14	0.14	0.00	0.08
1507	G 1352A	0.19	0.19	5.87	0.22	1.37	0.40	0.39	0.32	2.00	0.17	0.00	0.07
1529	G 1362	3.73	0.29	1.75	0.20	3.43	0.30	3.05	0.26	6.19	0.14	1.10	0.10
1530	G 1363	0.52	0.21	4.28	0.19	0.92	0.39	0.48	0.27	2.40	0.13	0.19	0.10
1611	G 1386	0.26	0.33	6.07	0.24	0.88	0.43	0.09	0.32	2.25	0.18	0.10	0.07
1616	G 1388	9.64	0.27	6.54	0.22	3.20	0.33	3.02	0.27	6.82	0.16	3.73	0.08
1657	G J 3612	0.03	0.27	6.20	0.24	0.88	0.44	0.51	0.31	2.38	0.16	0.13	0.09
1658	G 1398	10.40	0.25	9.03	0.23	5.79	0.34	6.10	0.31	10.66	0.17	5.14	0.09
1660	G J 3613	9.86	0.25	7.09	0.25	3.76	0.38	3.41	0.27	7.38	0.19	3.96	0.09
1690	G 1403	2.85	0.36	5.15	0.24	1.27	0.46	0.49	0.33	2.45	0.16	0.20	0.08
1742	G J 3647	9.41	0.32	9.25	0.27	7.10	0.38	6.43	0.36	11.08	0.19	5.39	0.08
1795	G J 3666	0.21	0.24	5.72	0.24	1.29	0.40	0.39	0.32	2.24	0.11	0.05	0.09
1838	G 1443	0.92	0.15	4.89	0.24	0.07	0.45	0.39	0.25	2.23	0.17	0.22	0.08
1845	G 1445	0.05	0.31	6.10	0.24	1.27	0.42	0.46	0.31	2.25	0.13	0.73	0.13
1931	G J 3719	9.95	0.21	8.29	0.25	6.88	0.47	5.37	0.26	10.16	0.16	4.83	0.09
1988	G 1480	0.59	0.20	5.28	0.22	1.37	0.37	0.34	0.32	2.05	0.16	0.05	0.08
2009	G 1486	0.17	0.24	5.68	0.32	1.68	0.58	0.36	0.33	1.75	0.16	0.01	0.09
2088	G J 3775	0.61	0.31	4.13	0.17	1.53	0.35	0.12	0.31	2.29	0.15	0.13	0.10
2094	G 1507B	0.26	0.33	4.41	0.21	1.56	0.39	0.51	0.31	2.40	0.18	0.13	0.09
2175	G J 3804	0.31	0.38	4.42	0.21	1.19	0.40	0.34	0.30	2.57	0.20	0.12	0.10
2300	G 1553.1	0.14	0.28	4.79	0.19	1.27	0.43	0.56	0.29	2.53	0.15	0.20	0.10
2310	G 1555	0.77	0.26	3.41	0.17	1.42	0.38	0.39	0.28	2.31	0.14	0.17	0.11
2399	G J 3892	0.40	0.29	4.93	0.20	1.37	0.34	0.43	0.30	2.41	0.18	0.24	0.09
2410	G 1581	0.08	0.32	4.82	0.17	1.58	0.38	0.50	0.31	2.36	0.18	0.17	0.08
2456	G J 3913	0.17	0.32	5.03	0.19	1.73	0.36	0.54	0.30	2.66	0.15	0.45	0.12
2472	G 1597	0.20	0.37	4.81	0.18	1.56	0.42	0.74	0.32	2.43	0.25	0.13	0.09
2567	G 1617B	0.63	0.28	4.58	0.19	1.35	0.36	0.53	0.31	2.31	0.19	0.27	0.08
2587	G J 3953	1.16	0.23	4.00	0.18	0.06	0.40	0.52	0.31	2.48	0.15	0.10	0.09
2599	G 1628	0.71	0.28	4.86	0.17	0.77	0.41	0.42	0.28	2.20	0.10	0.27	0.10
2660	G 1643	3.79	0.26	0.20	0.20	2.48	0.33	2.11	0.28	5.58	0.12	2.21	0.07
2661	G 1644A	0.44	0.51	4.34	0.26	0.58	0.45	0.69	0.37	2.33	0.14	0.14	0.10
2665	G J 1207	7.49	0.39	6.11	0.33	4.23	0.49	2.61	0.35	8.05	0.19	3.94	0.10
2700	G 1655	0.45	0.18	5.10	0.18	0.71	0.39	0.45	0.28	2.11	0.13	0.37	0.08
2712	G 1660A	0.56	0.24	5.22	0.22	1.29	0.44	0.78	0.36	2.22	0.16	0.08	0.09
2714	G J 3992	0.47	0.17	5.06	0.18	0.92	0.37	0.45	0.27	2.04	0.12	0.41	0.10
2717	G 1661A	0.06	0.28	5.88	0.21	0.97	0.41	0.60	0.29	2.50	0.16	0.34	0.09
2719	G J 1212	0.22	0.32	4.13	0.18	1.55	0.39	0.31	0.29	2.45	0.16	0.20	0.09
2744	G 1669A	4.45	0.25	0.58	0.17	1.36	0.30	0.94	0.31	4.42	0.14	1.48	0.12
2797	G 1687	0.14	0.14	4.77	0.27	1.35	0.39	0.76	0.41	3.00	0.15	0.23	0.11
2846	G J 4038	0.42	0.18	5.33	0.18	0.67	0.41	0.55	0.28	1.97	0.12	0.16	0.08
2849	G 1699	0.23	0.46	4.42	0.23	1.52	0.44	0.86	0.34	2.93	0.13	0.78	0.13
2851	G J 4040	1.13	0.24	4.19	0.20	0.17	0.43	0.16	0.33	2.30	0.15	0.15	0.08
2888	G J 4048	0.12	0.22	5.88	0.30	1.45	0.53	1.07	0.34	1.56	0.18	0.21	0.09
2895	G J 1226	0.13	0.20	6.07	0.25	0.68	0.47	1.14	0.37	1.76	0.16	0.09	0.09
2898	G 1712	0.09	0.34	5.53	0.22	1.34	0.38	0.69	0.31	2.76	0.13	0.19	0.10
2901	G J 4055	0.15	0.23	5.42	0.23	0.89	0.45	0.79	0.33	1.97	0.15	0.09	0.10
2916	G J 4062	0.66	0.22	4.72	0.22	1.22	0.46	0.45	0.34	1.77	0.14	0.13	0.09
2921	G J 4063	1.10	0.28	4.24	0.18	0.96	0.39	0.33	0.28	2.20	0.13	0.08	0.09
2924	G 1720B	0.29	0.26	5.04	0.20	1.28	0.40	0.43	0.30	2.10	0.12	0.13	0.10
2937	G J 4068	5.76	0.39	3.74	0.24	0.98	0.33	2.21	0.33	6.45	0.17	2.82	0.09
2940	G J 4070	0.21	0.19	5.50	0.19	0.84	0.40	0.43	0.28	2.18	0.12	0.14	0.07
2945	G 1725A	0.12	0.45	5.35	0.32	0.79	0.56	0.87	0.43	2.80	0.29	0.29	0.11
2946	G 1725B	0.10	0.26	5.98	0.21	0.28	0.47	0.58	0.32	2.28	0.13	0.12	0.07
2964	G J 4083	0.16	0.24	6.34	0.47	0.84	0.45	0.59	0.29	2.25	0.14	0.19	0.09
2976	G 1735	5.76	0.26	1.52	0.17	1.67	0.27	1.07	0.30	4.59	0.14	2.29	0.08
3013	G J 4098	0.22	0.31	4.89	0.18	1.31	0.40	0.44	0.30	2.49	0.16	0.49	0.10
3032	G J 9652A	10.77	0.27	9.09	0.22	4.26	0.30	4.19	0.29	9.71	0.18	5.40	0.11
3058	G J 4110	5.84	0.28	2.29	0.20	2.06	0.29	2.29	0.32	6.35	0.14	2.74	0.11
3306	G J 9721B	3.73	0.59	3.26	0.37	0.17	1.05	2.33	0.39	6.38	0.31	2.69	0.09

TABLE 4  
Equivalent Widths Measured from Echelle Data

[RHG 95]	Name	Ca II K <sub>ARCES</sub> (Å)	K <sub>2</sub> ARCES (Å)	H <sub>1</sub> ARCES (Å)	H <sub>2</sub> ARCES (Å)	Ca II K <sub>H IRES</sub> (Å)	K <sub>2</sub> H IRES (Å)	H <sub>1</sub> H IRES (Å)	H <sub>2</sub> H IRES (Å)
492	G 1109						0.35	0.03	0.24
836	G 1179						0.72	0.07	0.14
1089	G J 3412	0.20	0.04	0.28	0.03		0.00		
1094	G 1251	0.23	0.01	0.27	0.03	0.22	0.03	0.23	0.03
1126	G 1263	0.34	0.02	0.30	0.02				
1168	G 1273						0.26	0.04	0.17
1328	G J 2069A	2.25	0.26	2.51	0.03				
1501	G J 1125						0.17	0.04	0.19
1529	G 1362	1.65	0.10	0.53	0.03	1.68	0.28	0.54	0.01
1616	G 1388						4.93	1.79	2.26
1658	G 1398	2.71	0.19	3.23	0.03				
1690	G 1403	0.15	0.02	0.23	0.03				
1838	G 1443	0.46	0.08	0.30	0.03				
1845	G 1445						0.12	0.01	0.24
1988	G 1480	0.57	0.06	0.34	0.03				
2009	G 1486						0.17	0.02	0.16
2175	G J 3804						0.27	0.03	0.14
2310	G 1555	0.20	0.02	0.18	0.02				
2410	G 1581	0.09	0.01	0.22	0.02	0.19	0.05	0.21	0.04
2567	G 1617B						0.58	0.05	0.34
2587	G J 3953	0.67	0.07	0.10	0.02				
2599	G 1628	0.18	0.01	0.21	0.02	0.27	0.03	0.21	0.01
2660	G 1643	0.15	0.03	0.19	0.02				
2665	G J 1207	2.38	0.18	2.56	0.04				
2700	G 1655						0.28	0.03	0.27
2712	G 1660A	0.38	0.03	0.27	0.03				
2714	G J 3992						0.38	0.05	0.26
2797	G 1687						0.31	0.07	0.27
2851	G J 4040	0.48	0.05	0.21	0.02				
2921	G J 4063						0.61	0.07	0.19
2940	G J 4070						0.14	0.01	0.24
2945	G 1725A						0.15	0.04	0.23
2946	G 1725B						0.19	0.03	0.24
3013	G J 4098						0.18	0.02	0.24
3478	G 1849						0.42	0.19	0.34



TABLE 5  
Stars with UV and X-ray Measurements

[RHG 95]	Name	$F_{\text{ROSAT}}$	$F_{\text{MD89Xray}}$ LOG (ergs s <sup>-1</sup> cm <sup>-2</sup> Å <sup>-1</sup> )	$F_{\text{gII;MD89}}$	$F_{\text{gII;ACS}}$
492	G 1109	12.53			
876	G J 3333	12.54			
933	G 1206	11.39	11.43		12.56
941	G J 3356	12.74			
1168	G 1273	12.99		12.52	12.68
1184	G 1277B	11.14			
1328	G J 2069A	11.26			
1405	G J 3522	10.93			
1507	G 1352A	12.97			
1529	G 1362	11.96			
1616	G 1388	10.60	10.50	11.90	11.72
1658	G 1398	11.85			
1742	G J 3647	11.58			
2567	G 1617B	12.47			
2599	G 1628	12.82			
2660	G 1643	10.56			
2661	G 1644A	10.56	11.13		12.08
2665	G J 1207	11.66			
2717	G 1661A	12.56			
2744	G 1669A	11.35			
2797	G 1687	12.51			
2916	G J 4062	13.32			
2945	G 1725A	12.70			
2946	G 1725B	12.70			
2976	G 1735	11.00	11.59	12.17	12.24
3478	G 1849		12.67		13.03
3584	G 1873	10.40			11.92

